plan. This suggested that the age-related degradation of respiratory function leads to unstable erratic respiration, but that set-up uncertainty is a more influential factor than the patient's characteristics.

Tsunashima et al. investigated the continuous tumor motion in end-expiration and they reported an average internal motion of 1.4–2.6 mm, these were regarded as corresponding to the residual motion [31]. Proton beams in our facility are delivered every 2 s within 0.1 s after the trigger, and the respiratory wave period is normally 3–4 s. Therefore proton beams are delivered at once in a respiration cycle during usual treatment, when the respiratory waveform dropped below the threshold of 25% in the expiratory phase. However, proton beams are sometimes triggered repeatedly during end-expiration when the patient breathes slowly. In this study, intrafractional uncertainty was unexpectedly large on rare occasions (i.e., in patients No. 15, the average uncertainty was 0.6 mm, but the maximum was 5.0 mm). This unexpected uncertainty could have been caused by the residual motion of the liver.

The limitation of this study was the relation between the markers and the tumor, and short observation time. We have implanted markers adjacent to the tumor, not into the tumor, because of the risk of bleeding and spread of tumor cells when the marker is inserted into the hepatic tumor. Bedder et al. showed that the correlation between the marker and tumor was good when the marker was implanted close to the tumor (3.2 cm max) [21]. Considering the median distance of 3.9 cm between the marker and tumor center in this study and our previous good treatment outcomes for hepatocellular carcinoma, the markers may correlate well with the tumor [1–5].

In this study, observation time in one fraction was short. Thus, baseline drift, which can be as large as much as 20% of the normal breathing amplitude [32], is not considered. Many authors have suggested the advantage of breathing control in high-precision radiotherapy [9,33–35]. According to Guckenberger et al., baseline drift occurred 15–30 min after the start of the treatment and was reduced by body fixation and breathing control [14]. A tumor tracking system for proton therapy holds great promise in the future.

In conclusion, it was indicated that localization of the targets was more reproducibility in end-expiration than that in end-inspiration. Also, feasible and practical margin values were obtained. These should contribute accuracy of respiration synchronized proton radiotherapy for liver tumors.

Financial disclosure

Supported in part by a Grant-in-Aid for Yong Scientists (B) from the Ministry of Education, Culture, Sports, Science and Technology of the Japanese Government.

Conflict of interest notification

None of the authors have a conflict of interest regarding the work in the article.

Appendix A

We indicate that DR was taken $(1, 2, \ldots i, \ldots n_{j,k})$ times at each $(1.2, \ldots j, \ldots J_k)$ fraction, and a total of N_k DRs were obtained for each $(1, 2 \ldots, k, \ldots, K)$ patient ($K = 30$ in this study) during the expiration and inspiration phases. $N_{k,ex}$ and $N_{k,in}$ was calculated as

$$N_{k,ex} = \sum_j^{J_k} n_{ex,j,k}$$

$$N_{k,in} = \sum_j^{J_k} n_{in,j,k},$$

where "*ex*" and "*in*" indicate the expiration and inspiration phases, respectively.

The coordinates of the centroid of the observed markers at fraction '*j*' in the expiration and inspiration phase were obtained by each marker coordinate

$$\vec{M}_{ex,i,j,k} = (x_{ex,i,j,k}, y_{ex,I,j,k}, z_{ex.i,j,k}),$$

$$\vec{M}_{in,i,j,k} = (x_{in,i,j,k}, y_{in,I,j,k}, z_{in.i,j,k}).$$

Appendix B. Calculation of intrafractional error in the expiration and inspiration phase

The coordinate of the centroid ($\vec{C}$) of the observed markers in each of the expiration and inspiration phases was obtained.

$$\vec{C}_{ex,j,k} = (\bar{X}_{ex,j,k}, \bar{Y}_{ex,j,k}, \bar{Z}_{ex,j,k}) = \left(\frac{\sum_i^{n_{ex,j}} x_{ex,j,k}}{n_{ex,j,k}}, \frac{\sum_i^{n_{ex,j}} y_{ex,j,k}}{n_{ex,j,k}}, \frac{\sum_i^{n_{ex,j}} z_{ex,j,k}}{n_{ex,j,k}} \right)$$

$$\vec{C}_{in,j,k} = (\bar{X}_{in,j,k}, \bar{Y}_{in,j,k}, \bar{Z}_{in,j,k}) = \left(\frac{\sum_i^{n_{ex,j}} x_{ix,j,k}}{n_{in,j,k}}, \frac{\sum_i^{n_{ex,j}} y_{in,j,k}}{n_{in,j,k}}, \frac{\sum_i^{n_{ex,j}} z_{in,j,k}}{n_{in,j,k}} \right)$$

where "*ex*" and "*in*" indicate the expiration and inspiration phases, respectively.

The distance from the centroid to each marker was denoted by "*d*".

$$d_{ex,j,i,k} = \sqrt{|\vec{C}_{ex,j,k} - \vec{M}_{ex,j,k}|^2}$$

$$d_{in,j,i,k} = \sqrt{|\vec{C}_{in,j,k} - \vec{M}_{in,j,k}|^2}$$

The average distance (D) throughout all sessions for each patient was calculated as follows:

$$D_{ex,k} = \frac{\sum_j^{J_k} \sum_i^{n_j} d_{ex,j,i,k}}{N_{ex}} \quad D_{in,k} = \frac{\sum_j^{J_k} \sum_i^{n_j} d_{in,j,i,k}}{N_{in}}$$

Appendix C. Calculation of PTV margin

The planned marker coordinates with the isocenter-origin for the patient k was denoted by $DRR_k = (X_{DRR,k}, Y_{DRR,k}, Z_{DRR,k})$. The deviation of the planned coordinates ($\vec{P}$) for each patient from the observed coordinates for i times in j sessions during the expiration phase was as follows:

$$\vec{P}_{k,i,j} = \vec{DRR}_k - \vec{M}_{ex,i,j,k}$$
$$= (X_{DRR,k} - x_{ex,i,j,k}, Y_{DRR,k} - y_{ex,i,j,k}, Z_{DRR,k} - z_{ex,i,j,k})$$

The average of $\vec{P}$ for each patient was denoted by $\vec{S}$, which represents the systematic error for each patient.

$$\vec{S}_k = (s_{x,k}, s_{y,k}, s_{z,k}) = \left(\frac{\sum_j^{J_k} \sum_i^{nj} \vec{p}_{x,i,j,k}}{N_k}, \frac{\sum_j^{J_k} \sum_i^{nj} \vec{p}_{y,i,j,k}}{N_k}, \frac{\sum_j^{J_k} \sum_i^{nj} \vec{p}_{z,i,j,k}}{N_k} \right)$$

The group mean of the set-up variation averaged over all dose fractions for each patient was denoted by $\vec{\mu}$

$$\vec{\mu} = (\mu_x, \mu_y, \mu_z) = \left(\frac{\sum_k^K s_{x,k}}{K}, \frac{\sum_k^K s_{y,k}}{K}, \frac{\sum_k^K s_{z,k}}{K} \right)$$

The SD of the interpatient set-up error was denoted by $\sum$ [28,29].

$$\sum = \left(\sqrt{\frac{\sum_k^K (\vec{s}_{x,k} - \vec{\mu})^2}{K-1}}, \sqrt{\frac{\sum_k^K (\vec{s}_{x,k} - \vec{\mu})^2}{K-1}}, \sqrt{\frac{\sum_k^K (\vec{s}_{x,k} - \vec{\mu})^2}{K-1}} \right)$$

The SD of deviation from the treatment plan for each patient was denoted by σ_k, which represents the random error for each patient. Then, the root-mean-square of σ_k of the patient group was denoted σ [29,36]:

$$\sigma_k = (\sigma_{x,k}, \sigma_{y,k}, \sigma_{z,k}) = \left(\sqrt{\frac{\sum_j^{J_k} \sum_i^{n_j} (p_{x,i,j,k})^2}{N_k - 1}}, \sqrt{\frac{\sum_j^{J_k} \sum_i^{n_j} (p_{y,i,j,k})^2}{N_k - 1}}, \sqrt{\frac{\sum_j^{J_k} \sum_i^{n_j} (p_{z,i,j,k})^2}{N_k - 1}} \right)$$

$$\sigma = (\sigma_x, \sigma_y, \sigma_z) = \left(\sqrt{\frac{\sum_k^K (\sigma_{x,k})^2}{K}}, \sqrt{\frac{\sum_k^K (\sigma_{y,k})^2}{K}}, \sqrt{\frac{\sum_k^K (\sigma_{z,k})^2}{K}} \right)$$

Using Σ and σ, the PTV margins were calculated as $2\Sigma + 0.7\sigma$.

Appendix D. Supplementary data

Supplementary data associated with this article can be found, in the online version, at doi:10.1016/j.radonc.2011.05.009.

Reference

[1] Chiba T, Tokuuye K, Matsuzaki Y, et al. Proton beam therapy for hepatocellular carcinoma: a retrospective review of 162 patients. Clin Cancer Res 2005;11:3799–805.

[2] Hashimoto T, Tokuuye K, Fukumitsu N, et al. Repeated proton beam therapy for hepatocellular carcinoma. Int J Radiat Oncol Biol Phys 2006;65:196–202.

[3] Hata M, Tokuuye K, Sugahara S, et al. Proton beam therapy for hepatocellular carcinoma with portal vein tumor thrombus. Cancer 2005;104:794–801.

[4] Hata M, Tokuuye K, Sugahara S, et al. Proton irradiation in a single fraction for hepatocellular carcinoma patients with uncontrollable ascites. Technical considerations and results. Strahlenther Onkol 2007;183:411–6.

[5] Hata M, Tokuuye K, Sugahara S, et al. Proton beam therapy for aged patients with hepatocellular carcinoma. Int J Radiat Oncol Biol Phys 2007;69:805–12.

[6] Xi M, Liu MZ, Zhang L, et al. How many sets of 4DCT images are sufficient to determine internal target volume for liver radiotherapy? Radiother Oncol 2009;92:255–9.

[7] Linthout N, Bral S, Van de Vondel I, et al. Treatment delivery time optimization of respiratory gated radiation therapy by application of audio-visual feedback. Radiother Oncol 2009;91:330–5.

[8] Xi M, Liu MZ, Deng XW, et al. Defining internal target volume (ITV) for hepatocellular carcinoma using four-dimensional CT. Radiother Oncol 2007;84:272–8.

[9] Balter JM, Brock KK, Lam KL, et al. Evaluating the influence of setup uncertainties on treatment planning for focal liver tumors. Int J Radiat Oncol Biol Phys 2005;63:610–4.

[10] Balter JM, Brock KK, Litzenberg DW, et al. Daily targeting of intrahepatic tumors for radiotherapy. Int J Radiat Oncol Biol Phys 2002;52:266–71.

[11] Case RB, Moseley DJ, Sonke JJ, et al. Interfraction and intrafraction changes in amplitude of breathing motion in stereotactic liver radiotherapy. Int J Radiat Oncol Biol Phys 2010;77:918–25.

[12] Case RB, Sonke JJ, Moseley DJ, et al. Inter- and intrafraction variability in liver position in non-breath-hold stereotactic body radiotherapy. Int J Radiat Oncol Biol Phys 2009;75:302–8.

[13] Eccles C, Brock KK, Bissonnette JP, et al. Reproducibility of liver position using active breathing coordinator for liver cancer radiotherapy. Int J Radiat Oncol Biol Phys 2006;64:751–9.

[14] Guckenberger M, Sweeney RA, Wilbert J, et al. Image-guided radiotherapy for liver cancer using respiratory-correlated computed tomography and cone-beam computed tomography. Int J Radiat Oncol Biol Phys 2008;71:297–304.

[15] Kitamura K, Shirato H, Shimizu S, et al. Registration accuracy and possible migration of internal fiducial gold marker implanted in prostate and liver treated with real-time tumor-tracking radiation therapy (RTRT). Radiother Oncol 2002;62:275–81.

[16] Wagman R, Yorke E, Ford E, et al. Respiratory gating for liver tumors: use in dose escalation. Int J Radiat Oncol Biol Phys 2003;55:659–68.

[17] Wunderink W, Mendez Romero A, de Kruijf W, et al. Reduction of respiratory liver tumor motion by abdominal compression in stereotactic body frame, analyzed by tracking fiducial markers implanted in liver. Int J Radiat Oncol Biol Phys 2008;71:907–15.

[18] Wunderink W, Mendez Romero A, Seppenwoolde Y, et al. Potentials and limitations of guiding liver stereotactic body radiation therapy set-up on liver-implanted fiducial markers. Int J Radiat Oncol Biol Phys 2010;77:1573–83.

[19] Balter JM, Sandler HM, Lam K, et al. Measurement of prostate movement over the course of routine radiotherapy using implanted markers. Int J Radiat Oncol Biol Phys 1995;31:113–8.

[20] Crook JM, Raymond Y, Salhani D, et al. Prostate motion during standard radiotherapy as assessed by fiducial markers. Radiother Oncol 1995;37:35–42.

[21] Beddar AS, Kainz K, Briere TM, et al. Correlation between internal fiducial tumor motion and external marker motion for liver tumors imaged with 4D-CT. Int J Radiat Oncol Biol Phys 2007;67:630–8.

[22] McKenzie A, van Herk M, Mijnheer B. Margins for geometric uncertainty around organs at risk in radiotherapy. Radiother Oncol 2002;62:299–307.

[23] Stroom JC, de Boer HC, Huizenga H, et al. Inclusion of geometrical uncertainties in radiotherapy treatment planning by means of coverage probability. Int J Radiat Oncol Biol Phys 1999;43:905–19.

[24] Stroom JC, Heijmen BJ. Geometrical uncertainties, radiotherapy planning margins, and the ICRU-62 report. Radiother Oncol 2002;64:75–83.

[25] van Herk M, Remeijer P, Rasch C, et al. The probability of correct target dosage: dose-population histograms for deriving treatment margins in radiotherapy. Int J Radiat Oncol Biol Phys 2000;47:1121–35.

[26] Bijhold J, Lebesque JV, Hart AA, et al. Maximizing setup accuracy using portal images as applied to a conformal boost technique for prostatic cancer. Radiother Oncol 1992;24:261–71.

[27] Antolak JA, Rosen II. Planning target volumes for radiotherapy: how much margin is needed? Int J Radiat Oncol Biol Phys 1999;44:1165–70.

[28] de Boer HC, de Koste JR, Senan S, et al. Analysis and reduction of 3D systematic and random setup errors during the simulation and treatment of lung cancer patients with CT-based external beam radiotherapy dose planning. Int J Radiat Oncol Biol Phys 2001;49:857–68.

[29] de Boer HC, Heijmen BJ. A protocol for the reduction of systematic patient setup errors with minimal portal imaging workload. Int J Radiat Oncol Biol Phys 2001;50:1350–65.

[30] Nelson C, Starkschall G, Balter P, et al. Assessment of lung tumor motion and setup uncertainties using implanted fiducials. Int J Radiat Oncol Biol Phys 2007;67:915–23.

[31] Tsunashima Y, Sakae T, Shioyama Y, et al. Correlation between the respiratory waveform measured using a respiratory sensor and 3D tumor motion in gated radiotherapy. Int J Radiat Oncol Biol Phys 2004;60:951–8.

[32] Zhang T, Keller H, O'Brien MJ, et al. Application of the spirometer in respiratory gated radiotherapy. Med Phys 2003;30:3165–71.

[33] Dawson LA, Eccles C, Bissonnette JP, et al. Accuracy of daily image guidance for hypofractionated liver radiotherapy with active breathing control. Int J Radiat Oncol Biol Phys 2005;62:1247–52.

[34] George R, Ramakrishnan V, Siebers JV, et al. Investigation of patient, tumour and treatment variables affecting residual motion for respiratory-gated radiotherapy. Phys Med Biol 2006;51:5305–19.

[35] McNair HA, Brock J, Symonds-Tayler JR, et al. Feasibility of the use of the active breathing co ordinator (ABC) in patients receiving radical radiotherapy for non-small cell lung cancer (NSCLC). Radiother Oncol 2009;93:424–9.

[36] Bethesda M. International commission on radiation units and measurements. Prescribing, recording and reporting photon beam therapy (supplement to ICRU report 50). Bethesda: ICRU; 1999.

ELSEVIER

Int. J. Radiation Oncology Biol. Phys., Vol. 81, No. 4, pp. e601–e606, 2011

0360-3016/$ - see front matter

doi:10.1016/j.ijrobp.2011.02.041

HYPERFRACTIONATED CONCOMITANT BOOST PROTON BEAM THERAPY FOR ESOPHAGEAL CARCINOMA

Masashi Mizumoto, M.D.,*† Shinji Sugahara, M.D.,*†¶ Toshiyuki Okumura, M.D.,*† Takayuki Hashimoto, M.D.,*† Yoshiko Oshiro, M.D.,*† Nobuyoshi Fukumitsu, M.D.,*† Akira Nakahara, M.D.,‡ Hideo Terashima, M.D.,§ Koji Tsuboi, M.D.,*† and Hideyuki Sakurai, M.D.*†

*Proton Medical Research Center and Departments of †Radiation Oncology, ‡Gastroenterological Medicine, and §Surgery, University of Tsukuba, Tsukuba, Ibaraki, Japan; and ¶Tokyo Medical University Ibaraki Medical Center, Ibaraki, Japan

Purpose: To evaluate the efficacy and safety of hyperfractionated concomitant boost proton beam therapy (PBT) for patients with esophageal cancer.

Methods and Materials: The study participants were 19 patients with esophageal cancer who were treated with hyperfractionated photon therapy and PBT between 1990 and 2007. The median total dose was 78 GyE (range, 70–83 GyE) over a median treatment period of 48 days (range, 38–53 days). Ten of the 19 patients were at clinical T Stage 3 or 4.

Results: There were no cases in which treatment interruption was required because of radiation-induced esophagitis or hematologic toxicity. The overall 1- and 5-year actuarial survival rates for all 19 patients were 79.0% and 42.8%, respectively, and the median survival time was 31.5 months (95% limits: 16.7– 46.3 months). Of the 19 patients, 17 (89%) showed a complete response within 4 months after completing treatment and 2 (11%) showed a partial response, giving a response rate of 100% (19/19). The 1- and 5-year local control rates for all 19 patients were 93.8% and 84.4 %, respectively. Only 1 patient had late esophageal toxicity of Grade 3 at 6 months after hyperfractionated PBT. There were no other nonhematologic toxicities, including no cases of radiation pneumonia or cardiac failure of Grade 3 or higher.

Conclusions: The results suggest that hyperfractionated PBT is safe and effective for patients with esophageal cancer. Further studies are needed to establish the appropriate role and treatment schedule for use of PBT for esophageal cancer. © 2011 Elsevier Inc.

Proton beam therapy, Esophageal cancer, Hyperfractionated, Radiotherapy, Toxicity.

INTRODUCTION

Esophageal carcinoma is a common cancer in Japan. This disease can be treated with radiotherapy using a standard external beam schedule of 60 Gy in 30 fractions with concurrent chemotherapy using 5-fluorouracil and cisplatin (1). Ishikura *et al.* achieved a 5-year survival rate of 29% using this chemoradiotherapy schedule (2). We have shown that proton beam therapy (PBT) is also effective for patients with esophageal cancer (3, 4). In these reports, the patients were treated with PBT and X-rays, and the median total dose of combined X-ray and proton radiation was about 80 GyE. With PBT, irradiation of organs such as the heart, lungs, and spinal cord is reduced in comparison to three-dimensional conformal X-ray therapy and intensity-modulated radiation therapy (5–7), and severe late toxicity does not develop in these organs despite the use of high-dose irradiation (3, 4). However, irradiation of the normal esophagus around a tumor is unavoidable, and severe late toxicity may occur in the esophagus after PBT.

Hyperfractionated radiotherapy is a well-established technique for head-and-neck cancer and lung cancer (8, 9). Zhao *et al.* have shown that hyperfractionated radiotherapy is also effective for esophageal carcinoma and that the toxicity is tolerable (10, 11). In our institute, hyperfractionated PBT of 96.6 GyE in 56 fractions (1.65 GyE and 1.8 GyE/fraction) has been tried for supratentorial glioblastoma multiforme, with achievement of good efficacy without severe late toxicity (12). Thus, we hypothesized that hyperfractionated PBT for esophageal cancer may reduce late toxicity in the esophagus. In this report, we evaluate the efficacy

Reprint requests to: Hideyuki Sakurai, M.D., Proton Medical Research Center, University of Tsukuba, 1.1.1. Tennoudai, Tsukuba, Ibaraki, 305-8575 Japan. Tel: (+81) 29-853-7100; Fax: (+81) 29-853-7102; E-mail: hsakurai@pmrc.tsukuba.ac.jp

Supported in part by a Grant-in-Aid for Young Scientists (B) from the Ministry of Education, Culture, Sports, Science and Technology of the Japanese Government.

Conflict of interest: none.

Received Oct 25, 2010, and in revised form Feb 7, 2011. Accepted for publication Feb 17, 2011.

Table 1. Patient and tumor characteristics in cases treated with hyperfractionated proton beam therapy

Characteristics	Number
Age (y)	55–84 (median 70)
Sex	
M	18
F	1
Primary tumor size (cm)	
Median	6
Range	2–15
TNM stage	
T1N0	5
T1N1	1
T2N0	1
T2N1	2
T3N0	3
T3N1	4
T4N1	3

and safety of hyperfractionated PBT in patients with esophageal cancer.

METHODS AND MATERIALS

Patients

The study participants were 77 patients with carcinoma of the esophagus who were treated by photon radiotherapy and PBT at our hospital from January 1990 to December 2007 and met the following eligibility criteria for the study: *(1)* histologically confirmed diagnosis of carcinoma, *(2)* World Health Organization performance status of 0–2, *(3)* provision of written informed consent for treatment, and *(4)* absence of uncontrolled malignant disease. PBT was considered to be an experimental treatment, and patients who received PBT were mainly those who were difficult to treat with standard therapy such as surgery or chemoradiotherapy.

Of the 77 patients, 19 were treated with hyperfractionated concomitant boost PBT. These 19 patients comprised 18 men and 1 woman, and had a median age of 70 years old (range, 55–84 years). The primary tumor sizes were 2.0 to 15.0 cm (median, 6.0 cm). The clinical stages were T1N0M0 in 5 patients, T1N1M0 in 1, T2N0M0 in 1, T2N1M0 in 2, T3N0M0 in 3, T3N1M0 in 4, and T4N1M0 in 3. Histologically, 18 of the 19 patients had squamous cell carcinoma and 1 had adenocarcinoma. The characteristics of the 19 patients are shown in Table 1. Pretreatment tests included complete blood counts, liver function tests, esophagoscopy using the Lugol dye method (13), esophagography, chest X-rays, computed tomography of the chest and upper abdomen, and bronchoscopy when necessary. Endoesophageal ultrasonograpy was initially optional, but was performed for all patients (41 in total) from 2001. Bone scans were obtained when indicated.

Radiotherapy

Treatment planning was based on computed tomography images taken at 5-mm intervals with the patient in the treatment position. For PBT, the patient's position was adjusted before each treatment session based on fluoroscopy. A respiration-gated system was used from February 1992 when respiratory movements of the esophagus exceeded 5 mm (14). All patients were treated with a combination of 10-MV X-rays and protons.

To define the location of the tumor clearly on fluoroscopy, *in situ* fiducial markers (iridium chips 0.5 mm in diameter and 3.0 mm in length) were implanted endoscopically at the cranial and caudal boundaries of the primary tumor. The primary tumor and lymph node region received about 50 GyE of irradiation. The field encompassed the supraclavicular fossa when the tumor was located on the cephalic side of the carina. The nodes were included in the field when mediastinal nodal metastasis was suspected. The cephalic and caudal borders of the initial radiation field were 3 cm from the primary tumor, and the lateral borders of the field were 2 cm from the primary tumor. Proton beam boost therapy for a visible tumor was administered with a 1-cm margin in the craniocaudal and anteroposterior directions and a 5-mm margin laterally. The margin for the PTV was 1 cm in X-ray radiotherapy and 5 mm for PBT. Before 2001, we were able to perform PBT only for a limited time, and it was difficult to administer PBT in four to five fractions per week, in part because of machine maintenance time. Therefore, we had to use a large fraction size. From 2001, the use of PBT every weekday has been available at the Proton Medical Research Center. With this availability, we have been able to narrow the fraction size to reduce late toxicity. In 7 of the 19 patients who received hyperfractionated PBT, radiotherapy with X-rays of 45 Gy in 25 fractions (5 days per week) was delivered in the morning, and concomitant boost PBT of 13 GyE in 10 fractions (2 days per week) was delivered >6 hours after X-ray radiotherapy. Conventional PBT of 19.8 GyE in nine fractions was then delivered as a boost. The total dose of this schedule was 77.9 GyE. In 3 of the 19 patients, X-ray radiotherapy of 45 Gy in 25 fractions (5 days per week) was delivered in the morning, and concomitant boost PBT of 35 GyE in 25 fractions (5 days per week) was delivered >6 hours after X-ray radiotherapy. The total dose of this schedule was 80.0 GyE. In 3 other patients, X-ray radiotherapy of 25.2 Gy in 14 fractions (5 days per week) was delivered in the morning, and concomitant boost PBT of 23.1 GyE in 14 fractions (5 days per week) was delivered >6 hours after X-ray radiotherapy. Conventional PBT of 25.7 GyE in 13 fractions was then delivered as a boost. The total dose of this schedule was 74.0 GyE. The other 6 patients were treated with different schedules. The median total dose for all patients was 78.0 GyE. The relative biologic effectiveness of PBT was assumed to be 1.1 (15, 16).

Evaluation after treatment

Endoscopy or esophagography was used to evaluate the initial tumor response immediately after the completion of treatment and 1 month later. Follow-up endoscopies were performed every 3 months for the first 2 years and every 4 to 6 months thereafter or when necessary. Complete response was defined as complete disappearance of all detectable tumors, without development of a new lesion in the esophagus, as confirmed by another evaluation performed 4 or more weeks later. Partial response was defined as a reduction in the maximal diameter of the tumor of ≥50%. Local progression was defined as tumor regrowth in the radiation field in imaging with or without biopsy. Distant metastases were diagnosed by imaging alone in most cases. Morbidity was scored according to the criteria of the Radiation Therapy Oncology Group and the European Organization for Research and Treatment of Cancer (17).

Statistics

Statistical tests were performed using the Dr. SPSS II package (SPSS Inc., Chicago, IL). Overall survival was defined as the time interval between the start of treatment and the last follow-up when the patient was alive. Calculation of the local control rate was based on the date on which tumor progression was found or the time of the last examination in patients with no esophageal

tumor after treatment. Overall survival and local control curves were examined by the Kaplan-Meier method (18).

RESULTS

Toxicity

As of June 2010, 11 of the 19 patients had died. The other 8 patients were alive, and the median follow-up period for survivors was 111.3 months (range, 10.8–121.3 months). Eighteen of the 19 patients completed PBT. The treatment was stopped at 48 GyE in the other patient because of uncontrollable aspiration pneumonitis. The median treatment period was 48 days (range, 38–53 days).

Acute treatment-related toxicities were generally mild: 9 patients experienced Grade 1 dermatitis in the irradiated skin; 11 and 5 experienced acute esophagitis of Grades 1 and 2, respectively; and 1 developed Grade 3 esophagitis. This patient required intravenous hyperalimentation at the end of treatment. However, we continued PBT because the irradiated field in the PBT boost was narrow and we believed that the acute reaction was controllable. Immediately after endoscopy after PBT, 3 of 19 patients had ulcer and 4 had pseudomembranous inflammation. Only 1 patient had Grade 3 late esophageal toxicity 6 months after PBT. This patient had a refractory ulcer and died of liver disease 8 months after PBT. There were no other nonhematologic toxicities such as radiation pneumonia or cardiac failure of Grade 3 or more.

Local control and overall survival

The clinical courses of the 19 patients are shown in Table 2. The overall 1- and 5-year actuarial survival rates for all 19 patients were 79.0% and 42.8%, respectively (Fig. 1), and the median survival time was 31.5 months (95% limits: 16.7–46.3 months). Of the 11 deaths, 9 were due to the tumor, one was caused by liver disease, and one death occurred for an unknown reason.

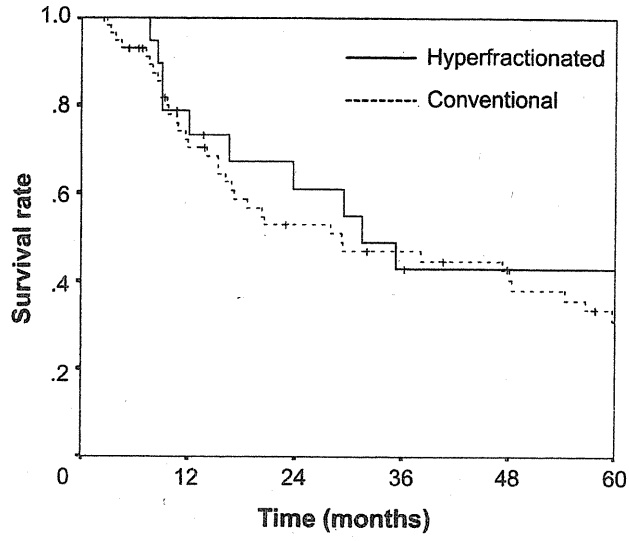

Fig. 1. Kaplan-Meier estimates of overall survival for patients with esophageal cancer treated with hyperfractionatedor conventional proton beam therapy.

Of the 19 patients, 17 (89%) showed a complete response within 4 months after completing treatment, and 2 (11%) showed a partial response, giving a response rate of 100% (19/19). Two patients had local recurrence at 7.0 and 17.7 months after PBT. The 1- and 5-year local control rates for all 19 patients were 93.8% and 84.4%, respectively

Table 2. Clinical course of 19 patients with esophageal carcinoma treated with hyperfractionated proton beam therapy

Patient	Age (y)	Sex	TMN classification	Tumor length (cm)	Tumor response	Pattern of recurrence	Overall survival (mo)	Follow-up and status
1	70	M	T1N0	8.0	CR	No recurrence	47.9	Alive
2	63	M	T1N0	2.0	CR	Local recurrence	35.2	Died of tumor
3	77	M	T1N0	2.0	CR	No recurrence	68.7	Alive
4	69	M	T1N1	3.0	CR	LN metastasis	63.5	Alive
5	80	M	T2N0	2.0	CR	No recurrence	10.8	Salvage surgery Alive
6	62	M	T1N0	5.0	CR	LN metastasis	31.5	Died of tumor
7	77	M	T3N1	7.0	CR	LN metastasis	12.1	Died of tumor
8	74	M	T2N1	8.0	CR	No recurrence	93.8	Alive
9	72	M	T3N0	10.0	CR	No recurrence	7.6	Died of liver disease
10	70	M	T3N1	5.0	CR	LN metastasis	23.8	Died of tumor
11	70	M	T3N0	5.0	CR	Esophageal recurrence*	116.5	Died of tumor
12	84	F	T3N0	6.0	CR	No recurrence	36.2	Alive
13	55	M	T4N1	4.0	CR	Lung metastasis	8.0	Died of tumor
14	60	M	T3N1	9.0	PR	Liver metastasis	15.3	Died of tumor
15	66	M	T3N1	7.0	CR	Bone metastasis	9.0	Died of tumor
16	58	M	T4N1	3.0	CR	No recurrence	121.3	Alive
17	80	M	T2N1	10.0	CR	No recurrence	13.7	Alive
18	72	M	T4N1	15.0	PR	Local recurrence	9.0	Died of tumor
19	79	M	T1N0	4.0	CR	Bone metastasis Lung metastasis	29.4	Died of unknown reason

Abbreviation: LN = lymph node.
* Esophageal recurrence; out-of-field esophageal recurrence. Primary tumor was controlled.

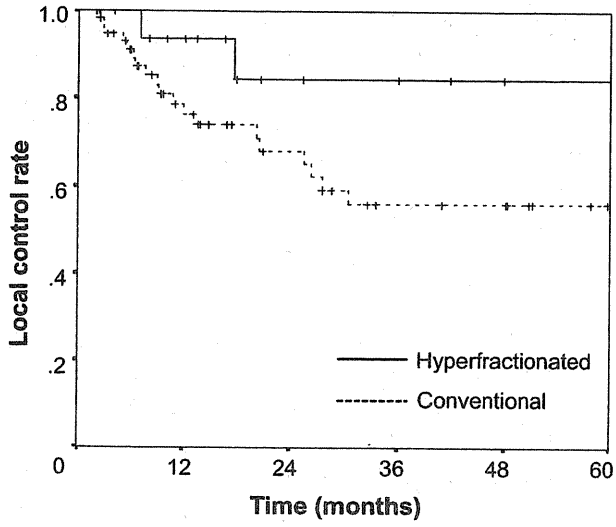

Fig. 2. Kaplan-Meier estimates of local control rates for patients with esophageal cancer treated with hyperfractionated or conventional proton beam therapy.

(Fig. 2). Eight patients (42%) remained disease progression-free at their last follow-up, but 11 (58%) had recurrence: 5 with distant metastases, 2 with recurrence at a lymph node inside the irradiated area of photon radiotherapy but outside the irradiated area of proton boost, 2 with metastasis to a lymph node outside the irradiated area, and 2 with primary recurrence.

Comparison of hyperfractionated PBT with conventional PBT

Of the 77 patients with esophageal cancer who were eligible for the study, 58 were treated by conventional proton and X-ray radiotherapy at our institute. The 58 patients comprised 53 men and 5 women and had a median age of 72 years (range, 45–95 years). The clinical stages were T1N0M0 in 26 cases, T1N1M0 in 7, T2N0M0 in 5, T2N1M0 in 1, T3N0M0 in 8, T3N1M0 in 8, and T4N0M0 in 3. The median total dose was 79.2 GyE (range, 61.6–89.0 GyE), and the median treatment period was 58 days (range, 44–77 days).

Acute treatment-related toxicities were generally mild: 26 patients experienced Grade 1 dermatitis in the irradiated skin; 36 and 5 experienced acute esophagitis of Grades 1 and 2, respectively; and 5 developed Grade 3 esophagitis. Fifteen patients had late esophageal toxicity of Grade 3 or higher. These late toxicity events occurred 3 to 36 months after PBT (median, 8 months). Six of the 15 patients had bleeding or esophageal perforation. The overall 1- and 5-year actuarial survival rates for all 58 patients were 70.4% and 46.7%, respectively (Fig. 1), and the median survival time was 29.2 months (95% limits: 7.2–51.1 months). The 1- and 5-year local control rates were 76.4% and 56.1 %, respectively (Fig. 2). A comparison of the characteristics and results of treatment with hyperfractionated and conventional PBT is shown in Table 3.

Table 3. Characteristics of patients with esophageal cancer treated by proton beam therapy (PBT)

Characteristics	Hyperfractionated PBT (n = 19)	Conventional PBT (n = 58)
T stage		
T1	6 (32%)	33 (57%)
T2	3 (16%)	6 (10%)
T3	7 (37%)	16 (28%)
T4	3 (16%)	3 (5%)
Treatment period (days)		
Median (range)	48 (38–53)	58 (44–77)
Total dose (GyE)		
Median (range)	78 (70–83)	79 (62–89)
Late toxicity (esophagus)		
Grade 3 or more	1 (5%)	14 (24%)
Histology		
Squamous	18 (95%)	57 (98%)
Adenocarcinoma	1 (5%)	0
Carcinoma	0	1 (2%)

DISCUSSION

The dose concentration in PBT allows irradiation at a high enough dose to control tumors that are difficult to treat with conventional radiotherapy (19–24). However, PBT for an esophageal tumor can result in severe toxicities such as esophagostenosis and esophageal ulcer. This problem may be addressed using hyperfractionated radiotherapy. In this study, we found that overall survival and local control after hyperfractionated PBT were as good as or better than after conventional PBT, even though the group of patients who underwent hyperfractionated PBT included several with advanced esophageal cancer. Most importantly, the rate of severe esophageal late toxicity (Grade 3 or more) was lower after hyperfractionated PBT (1/19, 5%) in comparison with conventional PBT (15/58, 26%).

Late toxicity of normal tissue is associated with fraction size (25, 26). The fraction size of hyperfractionated PBT was 1.8 GyE or less, and this small fraction size may have been an important factor in the low rate of late esophageal toxicity. We also found that late toxicity was mild despite the use of high-dose radiotherapy. The late toxicity of PBT is low in comparison with photon radiotherapy, and this is probably due to the excellent dose concentration in PBT. However, in this study the margin for PBT was only 5 mm, and the PTV margin was 1 cm or less. This treatment field was very narrow, and this may also have contributed to the mild late toxicity. Therefore, further investigation is needed to verify the factors associated with late toxicity of the esophagus after PBT.

Hyperfractionated radiotherapy is used to reduce the dose fraction without reducing the total dose targeting the tumor (8–12). We evaluated this approach in a clinical trial of hyperfractionated photon therapy and PBT for glioblastoma (12), in which photon therapy of 50.4 Gy in 28 fractions was administered in the morning and a proton beam boost of 46.2 GyE in 28 fractions was given more

than 6 hours after photon therapy. Thus, a high dose of irradiation of 96.6 GyE was given in 56 fractions over a relatively short treatment period of about 6 weeks, and the dose fraction was minimized. We consider that hyperfractionated PBT has two advantages. First, the treatment period may be reduced in comparison with conventional PBT, inasmuch as the median treatment periods in the current study were 48 days and 58 days for hyperfractionated and conventional PBT, respectively. Second, hyperfractionated PBT allows minimal irradiation of normal tissue while delivering almost the same total dose to the primary tumor.

Radiotherapy alone is currently not the standard therapy for esophageal cancer because it is inferior to chemoradiotherapy or surgery (27, 28). However, surgery or chemotherapy may not be suitable for patients whose condition is poor. To achieve good local control with radiotherapy alone has been difficult because of late toxicity of the lung, heart, and esophagus. However, we have shown that PBT for esophageal carcinoma minimizes irradiation of the lung, heart, and spinal cord and that patients treated by PBT do not develop severe late toxicity of these organs (3, 4). In addition, the current results indicate that hyperfractionated PBT has the potential to reduce esophageal toxicity.

In conclusion, we found that the efficacy of hyperfractionated PBT was equal to or better than that of conventional PBT in patients with esophageal cancer. Moreover, hyperfractionated PBT reduced the risk of esophageal late toxicity. Further studies are needed to establish the role and appropriate dosing schedule for use of PBT in treatment of esophageal cancer.

REFERENCES

1. Kenjo M, Uno T, Murakami Y, *et al.* Radiation therapy for esophageal cancer in Japan: Results of the Patterns of Care Study 1999-2001. *Int J Radiat Oncol Biol Phys* 2009;75:357–363.
2. Ishikura S, Nihei K, Ohtsu A, *et al.* Long-term toxicity after definitive chemoradiotherapy for squamous cell carcinoma of the thoracic esophagus. *J Clin Oncol* 2003;21: 2697–2702.
3. Sugahara S, Tokuuye K, Okumura T, *et al.* Clinical results of proton beam therapy for cancer of the esophagus. *Int J Radiat Oncol Biol Phys* 2005;61:76–84.
4. Mizumoto M, Sugahara S, Nakayama H, *et al.* Clinical results of proton beam therapy for locoregionally advanced esophageal cancer. *Strahlenther Onkol* 2010;186:482–488.
5. Zhang X, Zhao KL, Guerrero TM, *et al.* Four-dimensional computed tomography-based treatment planning for intensity-modulated radiation therapy and proton therapy for distal esophageal cancer. *Int J Radiat Oncol Biol Phys* 2008; 72:278–287.
6. Wang C, Nakayama H, Sugahara S, *et al.* Comparisons of dose-volume histograms for proton-beam versus 3-D conformal x-ray therapy in patients with stage I non-small cell lung cancer. *Strahlenther Onkol* 2009;185:231–234.
7. Macdonald OK, Kruse JJ, Miller JM, *et al.* Proton beam radiotherapy versus three-dimensional conformal stereotactic body radiotherapy in primary peripheral, early-stage non-small-cell lung carcinoma: A comparative dosimetric analysis. *Int J Radiat Oncol Biol Phys* 2009;75:950–958.
8. Bourhis J, Overgaard J, Audry H, *et al.* Hyperfractionated or accelerated radiotherapy in head and neck cancer: A meta-analysis. *Lancet* 2006;368:843–854.
9. Jenkins P, Anderson S, Wronski S, *et al.* A phase II trial of induction chemotherapy followed by continuous hyperfractionated accelerated radiotherapy in locally advanced non-small-cell lung cancer. *Radiother Oncol* 2009;93: 396–401.
10. Zhao KL, Shi XH, Jiang GL, *et al.* Late course accelerated hyperfractionated radiotherapy plus concurrent chemotherapy for squamous cell carcinoma of the esophagus: A phase III randomized study. *Int J Radiat Oncol Biol Phys* 2005;62:1014–1020.
11. Zhao KL, Shi XH, Jiang GL, *et al.* Late-course accelerated hyperfractionated radiotherapy for localized esophageal carcinoma. *Int J Radiat Oncol Biol Phys* 2004;60: 123–129.
12. Mizumoto M, Tsuboi K, Igaki H, *et al.* Phase I/II trial of hyperfractionated concomitant boost proton radiotherapy for supratentorial glioblastoma multiforme. *Int J Radiat Oncol Biol Phys* 2010;77:98–105.
13. Sugimachi K, Ohno S, Matsuda H, *et al.* Lugol-combined endoscopic detection of minute malignant lesions of the thoracic esophagus. *Ann Surg* 1988;208:179–183.
14. Tsunashima Y, Sakae T, Shioyama Y, *et al.* Correlation between the respiratory waveform measured using a respiratory sensor and 3D tumor motion in gated radiotherapy. *Int J Radiat Oncol Biol Phys* 2004;60:951–958.
15. Paganetti H, Niemierko A, Ancukiewicz M, *et al.* Relative biological effectiveness (RBE) values for proton beam therapy. *Int J Radiat Oncol Biol Phys* 2002;53:407–421.
16. Gerweck LE, Kozin SV. Relative biological effectiveness of proton beams in clinical therapy. *Radiother Oncol* 1999;50: 135–142.
17. Trotti A, Colevas AD, Setser A, *et al.* CTCAE v3.0: Development of a comprehensive grading system for the adverse effects of cancer treatment. *Semin Radiat Oncol* 2003;13: 176–181.
18. Kaplan EL, Meier P. Nonparametric estimation from incomplete observations. *J Am Stat Assoc* 1958;53:457–481.
19. Sugahara S, Oshiro Y, Nakayama H, *et al.* Proton beam therapy for large hepatocellular carcinoma. *Int J Radiat Oncol Biol Phys* 2010;76:460–466.
20. Mizumoto M, Tokuuye K, Sugahara S, *et al.* Proton beam therapy for hepatocellular carcinoma adjacent to the porta hepatis. *Int J Radiat Oncol Biol Phys* 2008;71:462–467.
21. Mizumoto M, Tokuuye K, Sugahara S, *et al.* Proton beam therapy for hepatocellular carcinoma with inferior vena cava tumor thrombus: Report of three cases. *Jpn J Clin Oncol* 2007;37: 459–462.
22. Nakayama H, Sugahara S, Tokita M, *et al.* Proton beam therapy for hepatocellular carcinoma: The University of Tsukuba experience. *Cancer* 2009;115:5499–5506.
23. Mizumoto M, Okumura T, Hashimoto T, *et al.* Proton beam therapy for hepatocellular carcinoma: A comparison of three treatment protocols. *Int J Radiat Oncol Biol Phys*. In press.
24. Nakayama H, Sugahara S, Tokita M, *et al.* Proton beam therapy for patients with medically inoperable stage I non-small-cell lung cancer at the University of Tsukuba. *Int J Radiat Oncol Biol Phys* 2010;78:467–471.
25. Thames HD Jr, Withers HR, Peters LJ, *et al.* Changes in early and late radiation responses with altered dose fractionation:

Implications for dose-survival relationships. *Int J Radiat Oncol Biol Phys* 1982;8:219–226.
26. Withers HR. Biologic basis for altered fractionation schemes. *Cancer* 1985;55:2086–2095.
27. Herskovic A, Martz K, al-Sarraf M, *et al.* Combined chemotherapy and radiotherapy compared with radiotherapy alone in patients with cancer of the esophagus. *N Engl J Med* 1992; 326:1593–1598.
28. Cooper JS, Guo MD, Herskovic A, *et al.* Chemoradiotherapy of locally advanced esophageal cancer. Long-term follow-up of a prospective randomized trial (RTOG 85-01). Radiation Therapy Oncology Group. *JAMA* 1999;281:1623–1627.

ELSEVIER

Int. J. Radiation Oncology Biol. Phys., Vol. 81, No. 4, pp. 1039–1045, 2011

0360-3016/$ - see front matter

doi:10.1016/j.ijrobp.2010.07.015

PROTON BEAM THERAPY FOR HEPATOCELLULAR CARCINOMA: A COMPARISON OF THREE TREATMENT PROTOCOLS

Masashi Mizumoto, M.D.,*† Toshiyuki Okumura, M.D.,*† Takayuki Hashimoto, M.D.,*† Kuniaki Fukuda, M.D.,‡ Yoshiko Oshiro, M.D.,*† Nobuyoshi Fukumitsu, M.D.,*† Masato Abei, M.D.,‡ Atsushi Kawaguchi, Ph.D.,§ Yasutaka Hayashi, M.D.,† Ayako Ookawa, M.D.,† Haruko Hashii, M.D.,† Ayae Kanemoto, M.D.,† Takashi Moritake, M.D.,*† Eriko Tohno, M.D.,‖ Koji Tsuboi, M.D.,*† Takeji Sakae, Ph.D.,* and Hideyuki Sakurai, M.D.*†

*Proton Medical Research Center, and Departments of †Radiation Oncology, ‡Gastroenterology, and ‖Diagnostic Radiology, University of Tsukuba, Tsukuba, Ibaraki, Japan; and §Biostatistics Center, Kurume University, Fukuoka, Japan

Background: Our previous results for treatment of hepatocellular carcinoma (HCC) with proton beam therapy revealed excellent local control with low toxicity. Three protocols were used to avoid late complications such as gastrointestinal ulceration and bile duct stenosis. In this study, we examined the efficacy of these protocols.
Methods and Materials: The subjects were 266 patients (273 HCCs) treated by proton beam therapy at the University of Tsukuba between January 2001 and December 2007. Three treatment protocols (A, 66 GyE in 10 fractions; B, 72.6 GyE in 22 fractions; and C, 77 GyE in 35 fractions) were used, depending on the tumor location.
Results: Of the 266 patients, 104, 95, and 60 patients were treated with protocols A, B, and C, respectively. Seven patients with double lesions underwent two different protocols. The overall survival rates after 1, 3 and 5 years were 87%, 61%, and 48%, respectively (median survival, 4.2 years). Multivariate analysis showed that better liver function, small clinical target volume, and no prior treatment (outside the irradiated field) were associated with good survival. The local control rates after 1, 3, and 5 years were 98%, 87%, and 81%, respectively. Multivariate analysis did not identify any factors associated with good local control.
Conclusions: This study showed that proton beam therapy achieved good local control for HCC using each of three treatment protocols. This suggests that selection of treatment schedules based on tumor location may be used to reduce the risk of late toxicity and maintain good treatment efficacy. © 2011 Elsevier Inc.

Proton beam therapy, Hepatocellular carcinoma, Survival, Local control, Radiotherapy.

INTRODUCTION

Hepatocellular carcinoma (HCC) is a common cancer in East Asia and Africa because of the high incidence of hepatic virus infection in these regions (1). The incidence of HCC in Japan is approximately 20 in 100,000 men and 10 in 100,000 women (2). Surgery, transcatheter arterial embolization (TAE), radiofrequency ablation (RFA), and hepatic transplantation are well established treatment modalities for HCC (3–16). In 1985, proton beam therapy (PBT) was started at the University of Tsukuba and has since resulted in good local control of HCC, with low toxicity (17). Nakayama *et al.* found that PBT was both safe and effective for HCC, and that liver function, T stage, performance status, and planned target volume had a significant influence on survival (18). The excellent dose distribution in PBT also makes it possible to treat HCC in unfavorable cases, such as elderly patients and those with large tumors, portal vein tumor thrombus, and poor liver function (19–26).

Kawashima *et al.* reported a 2-year local control rate of 96% in treatment with 76 GyE in 20 fractions (27), and found that a favorable liver function reserve (ICG R15) was related to good overall survival. At our hospital, three treatment protocols (66 GyE in 10 fractions, 72.6 GyE in 22 fractions, and 77 GyE in 35 fractions) are used, depending on the tumor location, to avoid late complications such as gastrointestinal ulceration and bile duct stenosis. Administration of 72.6 GyE in 22 fractions is applied mainly for HCC located adjacent to the porta hepatic, and 77 GyE in 35 fractions is used for HCC close to the intestinal tract. However, the optimal treatment schedule for HCC remains uncertain. Therefore, in the

Reprint requests to: Hideyuki Sakurai, M.D., Proton Medical Research Center, University of Tsukuba, Tennoudai, Tsukuba, Ibaraki, 305-8575 Japan. Tel: +81-29-853-7100; Fax: +81-29-853-7102; E-mail: hsakurai@pmrc.tsukuba.ac.jp

Supported in part by a Grant-in-Aid for Young Scientists (B) from the Ministry of Education, Culture, Sports, Science and Technology of the Japanese Government.

Conflict of interest: none.

Received April 26, 2010, and in revised form June 30, 2010. Accepted for publication July 1, 2010.

current study we examined the efficacy of PBT using the three different protocols.

METHODS AND MATERIALS

Patients

From September 2001 to November 2007, 266 patients with HCC met the following criteria for treatment with PBT: no active tumors outside the target volume; a performance status (PS) ≤2; hepatic function characterized by a Child-Pugh score ≤10; no extrahepatic metastasis; white blood cell count ≥1,000 /mm^3, hemoglobin level ≥6.5 g/dl, and platelet count ≥25,000/mm^3; and no uncontrolled ascites. Written informed consent was obtained from all patients before PBT.

The 266 patients comprised 193 men and 73 women, who had a median age of 70 years (range, 26–88 years). With regard to Eastern Cooperative Oncology Group (ECOG) performance status (PS), 159 patients were PS 0, 102 were PS 1, and 5 were PS 2. On the Child-Pugh classification for the degree of impairment of liver function, 203 patients were categorized as class A (scores 5–6), 60 as class B (scores 7–9), and 3 as class C (scores 10–12). In all, 25 patients were positive for hepatitis B virus (HBV), 193 for hepatitis C virus (HCV), and 6 for both HBV and HCV; 42 had neither type of infection. Of the 266 patients, 104 were treated with PBT using protocol A (66 GyE in 10 fractions), 95 using protocol B (72.6 GyE in 22 fractions), and 60 using protocol C (77 GyE in 35 fractions). Seven patients with double lesions were treated using two different treatment protocols.

There were 124 patients with a solitary mass and 142 with multiple tumors before PBT. The maximum tumor diameters ranged from 6 to 130 mm, with a median value of 34 mm. The clinical target volume (CTV) ranged from 2 to 1,398 cm^3, with a median volume of 49 cm^3. Of the 266 patients, 167 received another treatment (RFA, TAE, or surgery) before PBT. The normal liver volume was derived from the whole liver volume after deduction of the CTV, and ranged from 507 to 2,287 cm^3 (median, 1,068 cm^3). The characteristics of the patients and tumors are shown in Table 1.

Table 1. Characteristics of patients and tumors

Characteristic	*n**	%
Age (y)	26–88	70 (Median)
Sex		
Male	193	73
Female	73	27
ECOG performance status		
0	159	60
1	102	38
2	5	2
Etiology of liver disorder		
Hepatitis B virus	25	9
Hepatitis C virus	193	73
Both hepatitis B and C virus	6	2
No	42	16
Child-Pugh classification		
A	203	76
B	60	23
C	3	1
Treatment protocol		
Protocol A	104	39
Protocol B	95	36
Protocol C	60	23
Two protocols	7	3
Tumor size (mm)		
<30	100	38
30–49	96	36
50–99	62	23
≥100	8	3
Number of tumors		
Solitary	124	47
Multiple	142	53
Clinical target volume (cm^3)		
<20	78	29
20–49	56	21
50–99	53	20
100–199	42	16
≥200	37	14
Prior treatment		
Yes	167	63
No	99	37
Normal liver volume (cm^3)		
<700	16	6
700–999	96	36
1,000–1,249	86	32
1,250–1,499	44	17
≥ 1,500	24	9

Abbreviation: ECOG = eastern cooperative oncology group.
* Data are numbers and percentages unless otherwise indicated.

Pretreatment evaluation

All patients underwent blood tests, including complete blood cell counts, liver and renal function tests, and determination of electrolytes, hepatitis B and C virus titers, and α-fetoprotein (AFP). Abdominal computed tomography (CT) or magnetic resonance imaging (MRI) was used to evaluate the extent of HCC.

Proton beam therapy

The physical properties of our proton beams have been reported previously (28). Before treatment planning, patients had metallic fiduciary markers (iridium seeds of 0.8 mm in diameter and 2 mm in length) implanted in the vicinity of the tumor to aid in positioning. After making an individual immobilization cradle, CT images were taken at 5-mm intervals during the expiratory phase under a respiratory gating system (Anzai Medical Co., Tokyo, Japan) (29, 30). The CTV encompassed the gross tumor volume with a 5- to 10-mm margin in all directions. An additional 5-mm margin was included on the caudal axes to compensate for uncertainty resulting from respiration-induced hepatic movements. An additional margin of 5 to 10 mm was added to cover the entire CTV by enlarging the multileaf collimator and adjusting the range shifter. Proton beams from 155 to 250 MeV generated through a linear accelerator and synchrotron were spread out and shaped with ridge filters, double-scattering sheets, multicollimators, and a custom-made bolus to ensure that the beams conformed to the treatment planning data.

The proton beam schedule was selected depending on tumor location. A total dose of 77.0 GyE in 35 fractions (Protocol C) was selected for tumors within 2 cm of the gastrointestinal tract, 72.6 GyE in 22 fractions (Protocol B) was selected for tumors within 2 cm of the porta hepatis, and 66 GyE in 10 fractions (Protocol A) was selected for tumors that were not adjacent to the gastrointestinal tract or porta hepatis. The gastrointestinal tract was avoided as far as possible after 40 to 50 GyE. The relative biological effectiveness (RBE) of the PBT was assumed to be 1.1 (31).

The different radiation schedules were compared using the equivalent dose in 2-Gy fractions (EQD2) (32, 33), which takes into account the total dose and the dose per fraction. EQD2 is calculated from the following equation: EQD2 = D × [(d + α/β)/(2 Gy +α/β), where D is the total dose, d is the dose per fraction, α is the linear component of cell killing, β is the quadratic component of cell killing, and the α/β ratio is the effect on the tumor for 10 Gy. The EQD2 values were 78.3 GyE for Protocol C, 80.5 GyE for Protocol B, and 91.3 GyE for Protocol A, respectively.

Follow-up procedures and evaluation criteria

During treatment, acute treatment-related toxicities were assessed weekly in all patients. After completion of PBT, the patients were evaluated by physical examinations, CT or MRI, and blood tests every 3 months for the first 2 years and every 6 months thereafter. Local control was defined as no sign of regrowth or no new tumor in the treatment volume. For patients who died during follow-up, death was considered to be due to HCC in a case with marked progression of HCC or distant metastasis, and due to hepatic failure in a case with marked progression of coexisting liver cirrhosis without significant progression of HCC.

Statistical analysis

Overall and progression-free survival rates were evaluated in the 259 patients who received one treatment protocol. Local control was evaluated for 273 HCCs, including those in the 7 patients who received two different protocols. The Kaplan–Meier method was used for calculation of local control and survival rates, and a log-rank test was performed for evaluation of differences between two categories (34). The following potential prognostic factors were evaluated with respect to overall survival, progression-free survival and local control: age, liver function (Child-Pugh classification), PS, gender, hepatitis virus infection, prior treatment, number of tumors, treatment protocol, tumor size, CTV, and normal liver volume. Prior treatments were classified in-field and out-field. In-field was defined as prior treatment performed for HCC that included proton beam field, and out-field was defined has that which did not include proton beam field. Multivariate analyses were performed using a Cox proportional hazard model. At first univariate analysis was performed to the data including all factors. Multivariate analysis was performed to the selected factors, with p values in the univariate analysis being less than 0.2, and taking into account for thier correlations. Acute and late treatment-related toxicities were assessed using the National Cancer Institute Common Toxicity Criteria for Adverse Events v.3.0 (35) and the Radiation Therapy Oncology Group (RTOG)/European Organization for Research and Treatment of Cancer (EORTC) late radiation morbidity scoring scheme.

RESULTS

Patients

All but 1 patient who had a treatable intratumor hemorrhage completed PBT according to the treatment protocol, and all patients were followed up until death or until December 2009. At the time of analysis, 180 patients were alive, and 86 patients had died: 69 due to HCC, 9 due to hepatic failure, and 8 due to other causes.

Toxicity

Acute reactions were generally mild. Of the 266 patients, 127, 12, and 2 had radiation dermatitis of Grades 1, 2 and 3, respectively. Twelve patients had a symptomatic late toxicity: 3 had a rib fracture, 3 had dermatitis (2 patients of Grade 1 and 1 patient of Grade 3), and 6 had perforation, bleeding or inflammation of the digestive tract (3 of Grade 2, 3 of Grade 3).

Survival

The overall survival rates after 1, 3, and 5 years were 87% (95% confidence interval [CI], 83–92%), 61% (53–68%), and 48% (38–57%), respectively. The median overall survival period was 50.6 months (range, 39.1–62.1 months). There was no significant difference in overall survival between the three treatment protocols (Fig. 1). In univariate analysis of all the potential prognostic factors, CTV, normal liver volume, tumor size, Child-Pugh classification, prior treatment (out-field) and number of tumor were associated with survival. A p value for prior treatment (in-field) was less than 0.2. Among the selected factors noted above, the pairs of factors strongly associated with each other were tumor size and CTV; and number of tumor and prior treatment (out-field). Of the first pair, only CTV was significant; of the second pair, only prior treatment (out-field) was significant. Based on these results, tumor size and number of tumors were removed from the analysis. The Cox model was then fitted to the patient data using the selected factors (Table 2). Small CTV (<200 cc), good liver function, and no prior treatment (out-field) were significantly associated with good survival.

The progression-free survival rates after 1, 3, and 5 years were 56% (95% CI, 49–62%), 21% (15– 27%), and 12% (6– 18%), respectively. The median progression-free survival period was 13.5 months (range, 11.8– 15.2 months). In univariate analysis, of all the potential prognostic factors, CTV, Child-Pugh classification, prior treatment (out-field), and number of tumor were associated with progression-free survival. A p value for prior treatment (in-field), treatment

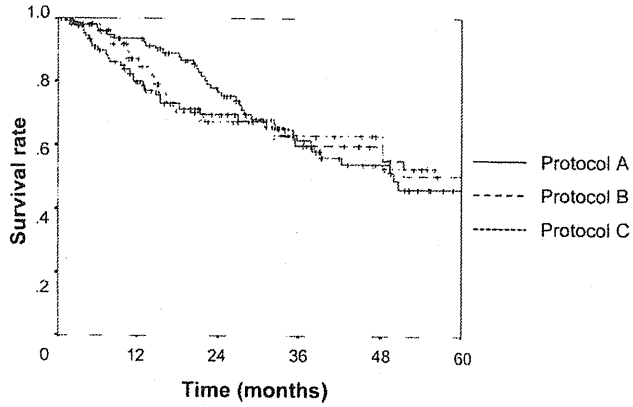

Fig. 1. Kaplan–Meier estimates of overall survival rates for 259 patients. There were no significant differences among the three treatment protocols.

Table 2. Multivariate analysis of potential predictive factors for overall survival

Factor	Patients (*n*)	3-Year OS	5-year OS	Multivariate *p*	HR	95% CI
CTV (cm^3)				0.001	4.29	2.51–7.33
<200	223	64.3	55.3			
≥200	36	37.5	7.8			
Normal liver volume				0.158	0.72	0.46–1.14
<1,000	109	54.4	39.5			
≥1,000	150	65.3	53.2			
Child-Pugh classification				0.001	2.37	1.42–3.94
A	198	65.7	55.1			
B or C	61	41.2	11.4			
Prior treatment (in-field)				0.284	1.28	0.82–2.01
No	119	69.5	57.5			
Yes	140	52.4	38.5			
Prior treatment (out-field)				0.002	2.10	1.33–3.31
No	171	69.4	51.5			
Yes	88	43.0	39.1			

Abbreviations: CI = confidence interval; HR = hazard ratio.

protocol, hepatitis, and tumor size was less than 0.2. Among selected factors, the pairs of factors strongly associated with each other were tumor size and CTV, and number of tumor and prior treatment (out-field). Of the first pair, only CTV was significant; of the second pair, only number of tumor was significant. Based on these results, tumor size and prior treatment (out-field) were removed from the analysis. The Cox model was then fitted to the patient data using the selected factors (Table 3). Small CTV (<200 cc), good liver function and solitary tumor were significantly associated with good progression free survival.

Local control

The 1-, 3-, and 5-year local control rates were 98% (95% CI, 96–100%), 87% (81–93%), and 81% (68–94%), respectively. There were no significant local control differences among the three treatment protocols (Fig. 2). In univariate analysis of all the potential prognostic factors, no single factor was associated with local control. A *p* value for tumor size, liver function and prior treatment (in-field) was less than 0.2. The Cox model was then fitted to the patient data using the selected factors (Table 4). In multivariate analysis, no factor was associated with local control.

DISCUSSION

Three treatment strategies are commonly used for HCC: curative treatment, transarterial chemoembolization, and systemic therapy using drugs such as sorafenib (36–40). Resection, RFA, and liver transplantation are classified as curative treatments. The recurrence-free survival after

Table 3. Multivariate analysis of potential predictive factors for progression-free survival (PFS)

Factor	Patients (*n*)	3-Year PFS	5-Year PFS	Multivariate *p*	HR	95% CI
CTV (cm^3)				0.001	2.16	1.41–3.29
<200	223	23.4	13.0			
≥200	36	7.7	7.7			
Hepatitis				0.10	1.44	0.94–2.23
No	41	29.7	11.9			
Yes	218	19.6	12.5			
Treatment protocol				0.224	1.14	0.92–1.40
Protocol A	104	21.6	19.9			
B	95	27.3	11.3			
C	60	9.5	0.0			
Child-Pugh classification				0.007	1.63	1.14–2.33
A	198	23.5	13.4			
B or C	61	13.8	13.8			
Prior treatment (in-field)				0.210	1.21	0.90–1.63
No	119	22.5	16.8			
Yes	140	18.3	9.3			
No. of tumors				0.001	1.82	1.34–2.47
Solitary	124	29.0	19.1			
Multiple	135	13.4	6.5			

Abbreviations: CI = confidence interval; CTV = clinical target volume; HR = hazard ratio.

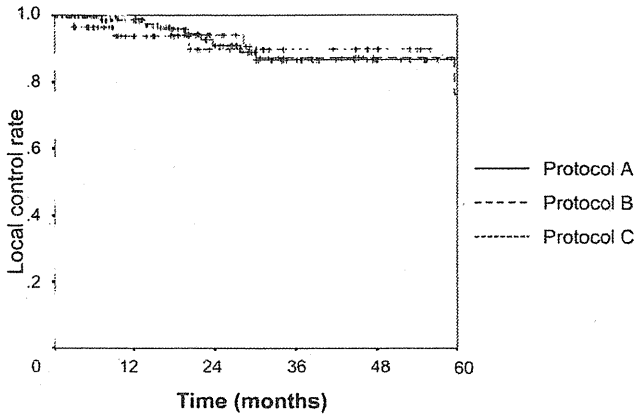

Fig. 2. Kaplan–Meier estimates of local control rates for 273 tumors. There were no significant differences among the three treatment protocols.

curative treatment is good, but the eligibility criteria are strict, with a requirement for a small number of tumors, relatively small tumors, and good liver function. Radiotherapy has yet to be established as a curative treatment, but several reports have shown limited success of radiotherapy for HCC (41–44). In these reports, the radiation dose was limited to about 50 Gy because of the potentially negative impact on critical organs such as the digestive tract, liver, and spinal cord. However, this dose is insufficient to achieve good local control compared to other curative treatment. Therefore, radiotherapy for HCC has been limited and has not been adopted as a standard therapy.

Our previous reports on proton beam therapy suggest that this approach has potential as a curative treatment for HCC (17–26). We mainly use three treatment protocols of 66 GyE in 10 fractions, 72.6 GyE in 22 fractions, and 77 GyE in 35 fractions. Kawashima *et al.* reported that PBT of 76 GyE in 20 fractions (EQD2 = 87.4 GyE) for HCC achieved good local control (27), and Bush *et al.* used 63 GyE in 15 fractions (EQD2 = 74.6 GyE) for HCC(45). In the current study, 77 GyE in 35 fractions was the lowest dose when $\alpha/\beta = 10$ was used, and the local control rates did not differ significantly between this protocol and the two other protocols (66 GyE in 10 fractions and 72.6 GyE in 22 fractions). The minimum dose to maintain good local control is uncertain, but this result indicates that a schedule of 77 GyE in 35 fractions is sufficient for this purpose. The 2-year local control rate of 75% in Bush et al. (63 GyE in 15 fractions, EQD2 = 74.6 GyE) is slightly lower than our data, which suggests that the minimum dose for HCC is close to 74 GyE. However, there are no definitive data that compared different doses of proton beam therapy for HCC. Further prospective trials are needed to clarify adequate doses for HCC. Tumor size and prior treatment were not associated with local control in our patients. Therefore, PBT may have a major role in treatment of both favorable (small, solitary tumors and good liver function) and difficult-to-treat cases of HCC, such as those with large tumors or a recurrent tumor after another curative therapy (21, 23, 25, 26).

Acute reactions were generally mild, and only 1 patient with a treatable intratumor hemorrhage was unable to complete the scheduled treatment. Perforation, bleeding, or inflammation of digestive tract was the most common symptomatic late toxicity. We routinely avoid irradiation of the digestive tract after 40 to 50 GyE, but it is difficult to avoid this completely because of setup errors and respiratory variation. To solve this problem, an additional device for real time monitoring of respiratory variation or surgical spacer placement may be useful. Regarding the treatment period, Protocol C took 7 to 8 weeks, which was too long. To shorten this period, another treatment strategy should be developed for irradiating tumor close to the gastrointestinal tract.

Progression-free survival was significantly associated with CTV, liver function, and number of tumors. The most common pattern of progression was recurrence outside the irradiated field, and the main cause of death after PBT was tumor-related. Therefore, the prognostic factors for overall survival were similar to those for progression-free survival, as also found in our previous reports (17–26). Treatment protocols were not associated with survival because the local control rate was already high, and no differences were found among the three protocols. There is probably little room for improvement of local control rate by dose escalation, which suggests that it may be more important to combine PBT with other treatment and reduce the toxicity without loss of efficacy.

Table 4. Multivariate analysis of potential predictive factors for local control (LC)

Factor	Patients (*n*)	3-Year LC	5-Year LC	Multivariate *p*	HR	95% CI
Tumor size (cm^3)				0.111	2.53	0.81–7.92
< 0	104	90.9	90.9			
≥30	169	84.8	78.2			
Child-Pugh classification				0.087	2.53	0.87–7.33
A	208	89.0	82.1			
B or C	65	79.1	79.1			
Prior treatment (in-field)				0.256	1.77	0.66–4.73
No	125	90.0	90.0			
Yes	148	84.7	74.1			

Abbreviations: CI = confidence interval; HR = hazard ratio.

CONCLUSION

In conclusion, each of the three treatment protocols had achieved high rates of local tumor control and excellent 5-year survival. The choice of fractionation schedule should continue to be based on the proximity of the dose limiting structures, such as porta hapatis and GI tract. If shorter courses of treatment may be possible for tumors near the GI tract, but it would require more advanced planning and delivery such as IGRT and active breathing control. PBT appears to be an effective curative option for HCC. Comparative trials are needed to assess the role of PBT compared with other locoregional modalites.

REFERENCES

1. Tanaka K, Hirohata T, Koga S, *et al.* Hepatitis C and hepatitis B in the etiology of hepatocellular carcinoma in the Japanese population. *Cancer Res* 1991;51:2842–2847.
2. Ajiki WKN, Tsukuma H, *et al.* Cancer incidence and incidence rates in Japan in 1995: Estimates based on data from nine population-based cancer registries. The Research Group for Population-based Cancer Registration in Japan. *Jpn J Clin Oncol* 2000;30:318–321.
3. Arii S, Yamaoka Y, Futagawa S, *et al.* Results of surgical and nonsurgical treatment for small-sized hepatocellular carcinomas: A retrospective and nationwide survey in Japan. The Liver Cancer Study Group of Japan. *Hepatology* 2000;32:1224–1229.
4. Chen MS, Li JQ, Zheng Y, *et al.* A prospective randomized trial comparing percutaneous local ablative therapy and partial hepatectomy for small hepatocellular carcinoma. *Ann Surg* 2006; 243:321–328.
5. Huang GT, Lee PH, Tsang YM, *et al.* Percutaneous ethanol injection versus surgical resection for the treatment of small hepatocellular carcinoma: A prospective study. *Ann Surg* 2005;242: 36–42.
6. Ikai I, Itai Y, Okita K, *et al.* Report of the 15th follow-up survey of primary liver cancer. *Hepatol Res* 2004;28:21–29.
7. Lencioni RA, Allgaier HP, Cioni D, *et al.* Small hepatocellular carcinoma in cirrhosis: Randomized comparison of radiofrequency thermal ablation versus percutaneous ethanol injection. *Radiology* 2003;228:235–240.
8. Mazzaferro V, Regalia E, Doci R, *et al.* Liver transplantation for the treatment of small hepatocellular carcinomas in patients with cirrhosis. *N Engl J Med* 1996;334:693–699.
9. Pacella CM, Francica G, Di Lascio FM, *et al.* Long-term outcome of cirrhotic patients with early hepatocellular carcinoma treated with ultrasound-guided percutaneous laser ablation: A retrospective analysis. *J Clin Oncol* 2009;27:2615–2621.
10. Poon RT, Fan ST, Lo CM, *et al.* Improving survival results after resection of hepatocellular carcinoma: A prospective study of 377 patients over 10 years. *Ann Surg* 2001;234:63–70.
11. Shibata T, Isoda H, Hirokawa Y, *et al.* Small hepatocellular carcinoma: Is radiofrequency ablation combined with transcatheter arterial chemoembolization more effective than radiofrequency ablation alone for treatment? *Radiology* 2009;252:905–913.
12. Shiina S, Teratani T, Obi S, *et al.* Nonsurgical treatment of hepatocellular carcinoma: From percutaneous ethanol injection therapy and percutaneous microwave coagulation therapy to radiofrequency ablation. *Oncology* 2002;62(Suppl 1):64–68.
13. Takayasu K, Arii S, Ikai I, *et al.* Prospective cohort study of transarterial chemoembolization for unresectable hepatocellular carcinoma in 8510 patients. *Gastroenterology* 2006;131:461–469.
14. Tateishi R, Shiina S, Teratani T, *et al.* Percutaneous radiofrequency ablation for hepatocellular carcinoma. An analysis of 1000 cases. *Cancer* 2005;103:1201–1209.
15. Wakai T, Shirai Y, Suda T, *et al.* Long-term outcomes of hepatectomy vs percutaneous ablation for treatment of hepatocellular carcinoma < or =4 cm. *World J Gastroenterol* 2006; 12:546–552.
16. Yoo HY, Patt CH, Geschwind JF, *et al.* The outcome of liver transplantation in patients with hepatocellular carcinoma in the United States between 1988 and 2001: 5-Year survival has improved significantly with time. *J Clin Oncol* 2003;21: 4329–4335.
17. Chiba T, Tokuuye K, Matsuzaki Y, *et al.* Proton beam therapy for hepatocellular carcinoma: A retrospective review of 162 patients. *Clin Cancer Res* 2005;11:3799–3805.
18. Nakayama H, Sugahara S, Tokita M, *et al.* Proton beam therapy for hepatocellular carcinoma: The University of Tsukuba experience. *Cancer* 2009;115:5499–5506.
19. Fukumitsu N, Sugahara S, Nakayama H, *et al.* A prospective study of hypofractionated proton beam therapy for patients with hepatocellular carcinoma. *Int J Radiat Oncol Biol Phys* 2009;74:831–836.
20. Hata M, Tokuuye K, Sugahara S, *et al.* Proton beam therapy for hepatocellular carcinoma with limited treatment options. *Cancer* 2006;107:591–598.
21. Hata M, Tokuuye K, Sugahara S, *et al.* Proton beam therapy for hepatocellular carcinoma with portal vein tumor thrombus. *Cancer* 2005;104:794–801.
22. Hata M, Tokuuye K, Sugahara S, *et al.* Proton beam therapy for aged patients with hepatocellular carcinoma. *Int J Radiat Oncol Biol Phys* 2007;69:805–812.
23. Mizumoto M, Tokuuye K, Sugahara S, *et al.* Proton beam therapy for hepatocellular carcinoma with inferior vena cava tumor thrombus: Report of three cases. *Jpn J Clin Oncol* 2007;37: 459–462.
24. Mizumoto M, Tokuuye K, Sugahara S, *et al.* Proton beam therapy for hepatocellular carcinoma adjacent to the porta hepatis. *Int J Radiat Oncol Biol Phys* 2008;71:462–467.
25. Sugahara S, Nakayama H, Fukuda K, *et al.* Proton-beam therapy for hepatocellular carcinoma associated with portal vein tumor thrombosis. *Strahlenther Onkol* 2009;185:782–788.
26. Sugahara S, Oshiro Y, Nakayama H, *et al.* Proton beam therapy for large hepatocellular carcinoma. *Int J Radiat Oncol Biol Phys* 2010;76:460–466.
27. Kawashima M, Furuse J, Nishio T, *et al.* Phase II study of radiotherapy employing proton beam for hepatocellular carcinoma. *J Clin Oncol* 2005;23:1839–1846.
28. Tsujii H, Tsuji H, Inada T, *et al.* Clinical results of fractionated proton therapy. *Int J Radiat Oncol Biol Phys* 1993;25:49–60.
29. Ohara K, Okumura T, Akisada M, *et al.* Irradiation synchronized with respiration gate. *Int J Radiat Oncol Biol Phys* 1989;17:853–857.
30. Tsunashima Y, Sakae T, Shioyama Y, *et al.* Correlation between the respiratory waveform measured using a respiratory sensor and 3D tumor motion in gated radiotherapy. *Int J Radiat Oncol Biol Phys* 2004;60:951–958.
31. Paganetti H, Niemierko A, Ancukiewicz M, *et al.* Relative biological effectiveness (RBE) values for proton beam therapy. *Int J Radiat Oncol Biol Phys* 2002;53:407–421.
32. Barendsen GW. Dose fractionation, dose rate and iso-effect relationships for normal tissue responses. *Int J Radiat Oncol Biol Phys* 1982;8:1981–1997.
33. Joiner MC, Van der Kogel AJ. The linear-quadratic approach to fractionation and calculation of isoeffect relationships. In: Steel GG, editor. Basic clinical radiobiology. New York: Oxford University Press; 1997. p. 106–112.

34. kaplan EL MP. Nonparametric setimation from incomplete observations. *J am Stat Assoc* 1958;31:457–481.
35. National Cancer Institute. National Cancer Institute Common Toxicity Criteria. Available at: http://ctep.cancer.gov/protocolDevelopment/electronic_applications/docs/ctcaev3.pdf. Accessed March 2010.
36. Faivre S, Raymond E, Boucher E, *et al.* Safety and efficacy of sunitinib in patients with advanced hepatocellular carcinoma: An open-label, multicentre, phase II study. *Lancet Oncol* 2009;10:794–800.
37. Poon D, Anderson BO, Chen LT, *et al.* Management of hepatocellular carcinoma in Asia: Consensus statement from the Asian Oncology Summit 2009. *Lancet Oncol* 2009;10:1111–1118.
38. Thomas MB, Morris JS, Chadha R, *et al.* Phase II trial of the combination of bevacizumab and erlotinib in patients who have advanced hepatocellular carcinoma. *J Clin Oncol* 2009; 27:843–850.
39. Vokes EE, Herndon JE 2nd, Crawford J, *et al.* Randomized phase II study of cisplatin with gemcitabine or paclitaxel or vinorelbine as induction chemotherapy followed by concomitant chemoradiotherapy for stage IIIB non-small-cell lung cancer: Cancer and leukemia group B study 9431. *J Clin Oncol* 2002; 20:4191–4198.
40. Yau T, Chan P, Ng KK, *et al.* Phase 2 open-label study of single-agent sorafenib in treating advanced hepatocellular carcinoma in a hepatitis B-endemic Asian population: Presence of lung metastasis predicts poor response. *Cancer* 2009;115: 428–436.
41. Koo JE, Kim JH, Lim YS, *et al.* Combination of transarterial chemoembolization and three-dimensional conformal radiotherapy for hepatocellular carcinoma with inferior vena cava tumor thrombus. *Int J Radiat Oncol Biol Phys* 2009.
42. McIntosh A, Hagspiel KD, Al-Osaimi AM, *et al.* Accelerated treatment using intensity-modulated radiation therapy plus concurrent capecitabine for unresectable hepatocellular carcinoma. *Cancer* 2009;115:5117–5125.
43. Shirai S, Sato M, Suwa K, *et al.* Feasibility and efficacy of single photon emission computed tomography-based three-dimensional conformal radiotherapy for hepatocellular carcinoma 8 cm or more with portal vein tumor thrombus in combination with transcatheter arterial chemoembolization. *Int J Radiat Oncol Biol Phys* 2010;76:1037–1044.
44. Zhang XB, Wang JH, Yan ZP, *et al.* Hepatocellular carcinoma with main portal vein tumor thrombus: Treatment with 3-dimensional conformal radiotherapy after portal vein stenting and transarterial chemoembolization. *Cancer* 2009;115:1245–1252.
45. Bush DA, Hillebrand DJ, Slater JM, *et al.* High-dose proton beam radiotherapy of hepatocellular carcinoma: Preliminary results of a phase II trial. *Gastroenterology* 2004;127:S189–S193.

J. Radiat. Res., 52, 536–537 (2011)

First In-situ Dose Calculation Report Using In-treatment Kilovoltage Cone-beam CT and In-treatment Linac Parameters during Volumetric Modulated Arc Therapy

Akira SAKUMI[1], Akihiko HAGA[1], Satoshi KIDA[1], Naoya SAOTOME[1], Yukari OKANO[1], Kenshiro SHIRAISHI[1], Takeshi ONOE[1], Kiyoshi YODA[2], Kuni OHTOMO[1] and Keiichi NAKAGAWA[1]*

In-situ dose calculation/In-treatment cone-beam CT/Volumetric modulated arc therapy.

To the editor

Tumor registration using kilovoltage (kV) cone-beam CT (CBCT) prior to radiotherapy has been increasingly adopted for daily clinical practice. Compared to traditional two-dimensional bone registration, kV CBCT provides three-dimensional tumor registration between previously acquired planning CT and the CBCT on each treatment day. In addition, kV CBCT shows daily displacement and deformation of organs as well as regression of tumors during the course of the treatment.

As a natural next step, patient dose distribution on each treatment day has been gradually highlighted by using CBCT image data. The reported accuracy of the CBCT-based dose calculation in reference to a planning CT was within 2 to 3%.[1,2] In the meantime, we have already reported clinical kV CBCT imaging during rotational radiotherapy using a linac with a CBCT unit (Elekta, UK)[3] and volumetric modulated arc therapy (VMAT).[4] We also published a dose calculation procedure by referring to log files including actual data of multi leaf collimator (MLC) positions, jaw positions, gantry angles and MUs with an interval of every 0.25 seconds in the linac service mode.[5] Recently, Qian calculated dose distributions by combining CBCT images acquired before treatment and actual in-treatment log files stored in a Varian linac.[6] In contrast, we report the first in-situ dose calculation using in-treatment CBCT and in-treatment linac parameters during VMAT delivery, which may directly correspond to the actually absorbed dose distributions during treatment.

A treatment planning system (TPS), Pinnacle3 9.0 SmartArc (Phillips, Holland) was employed to create a single-arc VMAT plan for a prostate cancer patient. The PTV dose prescription (D_{95}) was 76 Gy in 38 fractions. The linac photon energy was 6 MV. A record and verify system, Mosaiq 1.6 (Elekta, USA), was employed with a linac control software, Desktop Pro 7.0.1 (Elekta, UK). A single-arc VMAT required approximately 120 seconds. During the VMAT delivery, a log file was recorded via iCOM interface (Elekta, UK). Subsequently, the iCom data format was converted to Pinnacle data format, thereby allowing Pinnacle to read actual MLC positions, jaw positions, gantry angles and MUs with an interval of every 0.25 seconds. During the VMAT delivery, in-treatment kV projection data were also stored and CBCT image reconstruction was performed by in-house software. By exporting these data back to the TPS, in-treatment dose distributions were obtained.

Figure 1(a) shows the resulting in-situ dose distribution calculated by the in-treatment CBCT and the in-treatment linac parameters. The innermost two contours are clinical target volume (CTV) and planning target volume (PTV) of the prostate cancer. A PTV margin of 5 mm was employed except for the rectum side with a 4 mm margin. The isodose contour lines are, from inside to outside, 107% (a tiny blue island near the PTV boundary), 95%, 90%, 80%, 70%, 60%, 50%, 30% and 10% (purple) of the prescribed dose. A CBCT value to density conversion table was created by referring to a planning CT value to density table at the corresponding pixel locations on the paired data set of the planning CT and the CBCT, in regions close to the PTV including prostate, fat, and bone anatomies. To reduce scattering effects, CBCT values were corrected, with a simple approximation, based on a reconstructed CBCT image of a water column phantom, where a non-linear correction function was determined as a function of radius from the image center. The calculated mean doses for the PTV and rectum using the planning CT and the CBCT agreed within 1.4% and 3.4%, respectively. Figure 1(b) shows in-situ isodose color map overlaid on the in-treatment CBCT image, and Fig. 1(c) shows dose distributions calculated by the planning

*Corresponding author: Phone: +81-3-5800-8786,
Fax: +81-3-5800-8786,
E-mail: k-nak@fg7.so-net.ne.jp
[1]Department of Radiology, University of Tokyo Hospital, 7-3-1 Hongo, Bunkyo-ku, Tokyo, 113-8655, Japan; [2]Elekta KK, 3-9-1 Shibaura, Minato-ku, Tokyo 108-0023, Japan.
doi:10.1269/jrr.11061

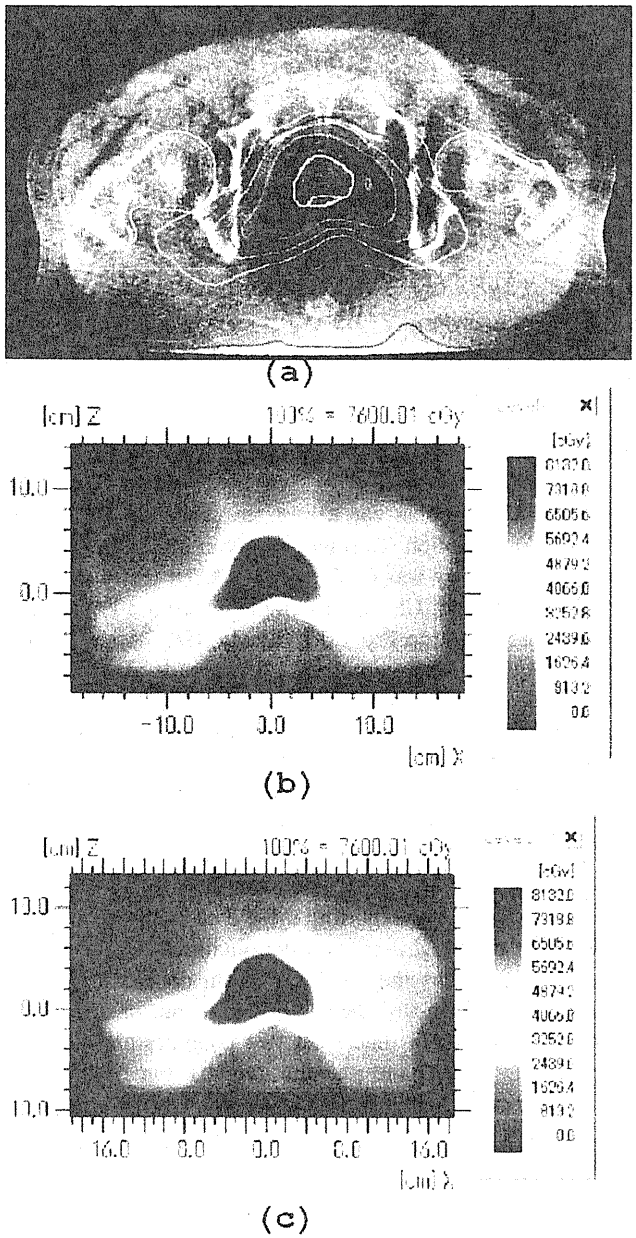

Fig. 1. In-situ dose calculation results using in-treatment cone-beam CT and in-treatment linac parameters during volumetric modulated arc therapy: (a) with isodose contours and (b) with isodose color map. An isodose color map calculated by the planning CT is shown in (c) for comparison.

CT for comparison. The pass rate of 1% dose difference between the dose distributions shown in (b) and (c) within the entire CBCT volume was 93.1%, whilst the pass rate of 2% dose difference went up to 96.5%. A reasonably good agreement was observed even if the body contour shapes were significantly different as shown at the both sides near the couch top.

In conclusion, we have shown that in-situ dose calculation during VMAT delivery is feasible by using in-treatment kV CBCT and in-treatment linac parameters. Further quantitative analysis is required to apply this technique to the next generation dose guided radiotherapy, which was originally proposed back in 2002.[7]

REFERENCES

1. Ding GX, *et al* (2007) A study on adaptive IMRT treatment planning using kV cone-beam CT. Radiother Oncol **85**: 116–125.
2. Richter A, *et al* (2008) Investigation of the usability of cone beam CT data sets for dose calculation. Radiation Oncology **3**: 42.
3. Nakagawa K, *et al* (2007) Verification of in-treatment tumor position using kilovoltage cone-beam computed tomography: preliminary study. Int J Radiat Oncol Biol Phys **69**: 970–973.
4 Nakagawa K, *et al* (2009) First clinical cone-beam CT imaging during volumetric modulated arc therapy. Radiother Oncol **90**: 422–423.
5. Haga A, *et al* (2009) Quality assurance of volumetric modulated arc therapy using Elekta Synergy. Acta Oncol **48**: 1193–1197.
6. Qian J, *et al* (2010) Dose reconstruction for volumetric modulated arc therapy (VMAT) using cone-beam CT and dynamic log files. Phys Med Biol **55**: 3597–3610.
7. Wu C, *et al* (2002) Re-optimization in adaptive radiotherapy. Phys Med Biol **47**: 3181–3195.

Received on April 11, 2011
Accepted on May 6, 2011

Radiotherapy and Oncology 100 (2011) 380–385

Contents lists available at SciVerse ScienceDirect

Radiotherapy and Oncology

journal homepage: www.thegreenjournal.com

Cone beam CT

4D-CBCT reconstruction using MV portal imaging during volumetric modulated arc therapy

Satoshi Kida, Naoya Saotome, Yoshitaka Masutani, Hideomi Yamashita, Kuni Ohtomo, Keiichi Nakagawa, Akira Sakumi, Akihiro Haga *

Department of Radiology, University of Tokyo Hospital, Japan

ARTICLE INFO

Article history:
Received 23 July 2011
Received in revised form 29 August 2011
Accepted 30 August 2011
Available online 29 September 2011

Keywords:
CBCT
4D-CT
Respiratory motion
Portal imaging
VMAT

ABSTRACT

Background: Recording target motion during treatment is important for verifying the irradiated region. Recently, cone-beam computed tomography (CBCT) reconstruction from portal images acquired during volumetric modulated arc therapy (VMAT), known as VMAT-CBCT, has been investigated. In this study, we developed a four-dimensional (4D) version of the VMAT-CBCT.

Materials and methods: The MV portal images were sequentially acquired from an electronic portal imaging device. The flex, background, monitor unit, field size, and multi-leaf collimator masking corrections were considered during image reconstruction. A 4D VMAT-CBCT requires a respiratory signal during image acquisition. An image-based phase recognition (IBPR) method was performed using normalised cross correlation to extract a respiratory signal from the series of portal images.

Results: Our original IBPR method enabled us to reconstruct 4D VMAT-CBCT with no external devices. We confirmed that 4D VMAT-CBCT was feasible for two patients and in good agreement with in-treatment 4D kV-CBCT.

Conclusion: The visibility of the anatomy in 4D VMAT-CBCT reconstruction for lung cancer patients has the potential of using 4D VMAT-CBCT as a tool for verifying relative positions of tumour for each respiratory phase.

 Radiotherapy and Oncology 100 (2011) 380–385

Radiotherapy is complex and verification of treatment is crucial. Although portal images acquired during treatment with an electronic portal imaging device (EPID) have been used as a planar image guidance tool and for geometrical quality assurance, the recent development of EPID dosimetry has provided in vivo dosimetry verification [1–3]. A Linac-mounted kV-CBCT is a powerful tool for verifying anatomical positions [4,5]. Accompanying rotational treatment such as volumetric modulated arc therapy (VMAT), in-treatment kV-CBCT images that reflect the patient's treatment position can be acquired just after the treatment [6–8]. The four-dimensional (4D) version known as 'in-treatment 4D kV-CBCT' verifies the positions of targets, such as lung tumours, with respiratory motion [9]. Acquiring CBCT images during treatment requires an orthogonal imager and a Linac-mounted kV source, and the isocentre displacement of the kV beam from the treatment beam must be carefully considered. More importantly, in-treatment kV-CBCT could expose the patient to additional radiation.

Recently, CBCT reconstruction with portal images during VMAT or VMAT-CBCT has been investigated [10]. The advantages of VMAT-CBCT are (1) no additional radiation exposure and (2) reduced hardware requirements, making the VMAT-CBCT a promising tool for verification of irradiated areas and/or in vivo dosimetry.

The 4D version of CBCT still presents a problem in acquiring respiratory signals for portal images. Generally, there are two methods to synchronously measure a respiratory signal with image acquisition. One method uses an image-based phase recognition (IBPR) technique [11–13]. The other uses an external respiratory monitoring system (e.g. AZ-733V by Anzai Medical Cooperation and real-time position management by Varian Medical System) [14]. This study tested the IBPR technique. For kV-CBCT, a technique of tracking small regions through the time series of projection images based on a maximum normalised cross correlation (NCC) was developed [9]. With this technique, parameters such as the size of the area were adjusted for application to portal images.

This paper reports on the feasibility of using 4D VMAT-CBCT as a treatment verification tool in two lung cancer patients receiving VMAT. Validity was assessed by comparing the tumour positions between 4D VMAT-CBCT images and in-treatment 4D kV-CBCT images simultaneously acquired during VMAT delivery. The 4D VMAT-CBCT images were also evaluated with phantom testing.

* Corresponding author. Address: Department of Radiology, The University of Tokyo Hospital, 7-3-1 Hongo, Bunkyo-ku, Tokyo 113-8655, Japan.
E-mail address: haga-haga@umin.ac.jp (A. Haga).

0167-8140/$ - see front matter © 2011 Elsevier Ireland Ltd. All rights reserved.
doi:10.1016/j.radonc.2011.08.047

Methods and materials

Outlook of the 4D VMAT-CBCT reconstruction process

4D VMAT-CBCT reconstruction is performed as follows: VMAT for lung cancer was delivered with an Elekta Synergy accelerator operating at 6 MV. During beam delivery, portal images were sequentially collected by EPID with an interval of 0.46 s using Elekta iViewGT software. The portal image consists of 1024 × 1024 pixels with a size of 0.25 mm at the isocentre. At maximum, 256 projection images per reconstruction were obtained. In order to connect the portal images with the corresponding gantry angles, we employed a log file via the Elekta software protocol, iCom, which records the gantry angle information during treatment. This was followed by matching the multi-leaf collimator (MLC) shapes derived from the portal images with those from iCom.

The acquired portal images can include the shift due to the geometric non-idealities in the rotation of the gantry system. The geometric non-idealities were measured in advance for gantry angle intervals of 5 degrees by analysing 10 cm × 10 cm radiation fields; this correction (flex correction) was performed for each portal image. The response of EPID was also regularised by considering the background (BG), linearity of monitor unit (MU), and field size (output factor) effects. MLC masking correction was performed according to Poludniowski et al. [10]. The MLC masking correction extrapolates the data truncated by the MLC field shape to mitigate artifacts otherwise induced by the filter operation of the CBCT reconstruction algorithm. A value in the masked region can be adjusted arbitrarily if we are interested only in visual images, not quantitative densities, within the patient. We defined the masking factor as a ratio of the maximum pixel value. In this study, we applied masking factors of 0.56 and 0.76 for patients 1 and 2, respectively.

Reconstruction of 4D VMAT CT requires a respiratory phase in the system. In this study, portal-image based phase recognition (P-IBPR) was employed using NCC (see below). The periodic selection of portal images of only one specific respiratory phase enables image reconstruction for that phase. Projection images were classified into 4 phases and the reconstructions were performed with a filtered back-projection (FBP) algorithm. The sequential process was performed off-line.

Portal-image based phase recognition (P-IBPR)

The method proposed here employs NCC with limited areas between adjacent portal images. Several rectangular areas ($w \times h = 5 \times 100$ pixels) are placed sequentially within exposed fields on each frame of the portal images to account for tumour motion. While a rectangular area in the current frame is fixed, an area on the next frame is moved so that the NCC value of the two areas is maximised. Movement is limited to the cranio-caudal axis. The position of the rectangular area was set to the initial position with respect to each portal image (see Fig. 1). By performing

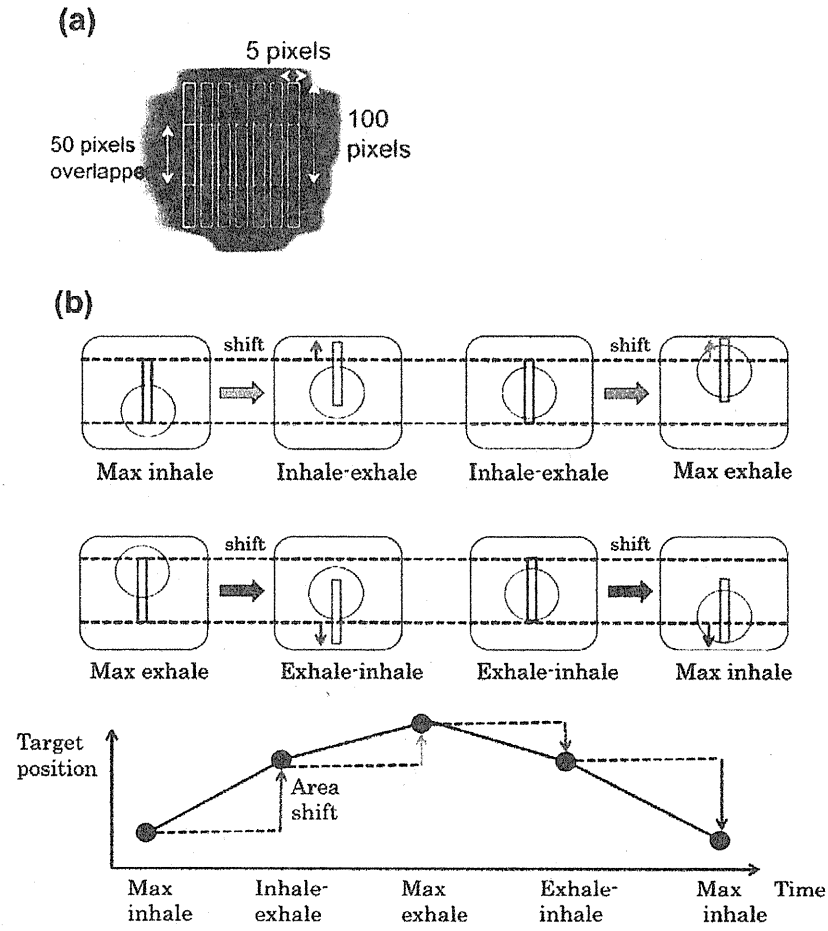

Fig. 1. (a) The distribution of several rectangular areas ($w \times h = 5 \times 100$ pixels) to cover tumour motion within exposed fields on each portal image. They are partially overlapped. (b) Schematic explanation of P-IBPR using NCC. The positions of the rectangular areas are shifted only along the cranio-caudal axis on the next portal image to find the maximum value of NCC with the calculation area on the previous portal image. The position of the rectangular area was set to the initial position with respect to each portal image. For the above example, the black rectangles indicate initial position and red rectangles indicate the position that gives the maximum NCC value with the corresponding black rectangles.

this procedure repeatedly for all portal images, a respiration signal can be obtained by displacement in the cranio-caudal direction. The signals were averaged among the calculation areas. Finally, low periodic components more than 5 s and high periodic components less than 1 s were removed in the frequency domain by using the band pass filter. The phase distributions were phase 0% (max inhale), phase 25% (inhale–exhale), phase 50% (max exhale), and phase 75% (exhale–inhale).

The efficiency of P-IBPR was determined by comparing the breathing pattern acquired by P-IBPR with those measured by visual tracking of the tumour on portal images. Here, the breathing cycle period was defined as the interval between adjacent max-expiration phases. In the visual tracking, a slight shaking can be recognised as a peak of expiration. Therefore, respirations with amplitudes less than 1 mm were neglected in the detection of max exhale.

Treatment planning for VMAT

One potential problem when inverse planning for lung cancer treatment is that the optimisation of beam fluences only takes into account a single three-dimensional volumetric data set. For this, the actual VMAT that continuously delivers the dose in all respiratory phases, may yield a dose distribution that differs from the plan. In order to compensate for this fact, the target volume can be extended to encompass the range of target motion by using 4D-CT scan, and field shapes can be defined as the target surroundings. Alternatively, the inverse plan that constrains MLC motion in VMAT forms field shapes that do not hide the target in lung cancer treatment. In this case, the beam intensity is mainly modulated by changing gantry speed and dose rate.

In this study, the planning target volume (PTV) for the lung tumour was created with a 5-mm margin of internal target volume generated from 20 4D-CT sets by using a 320-slice volumetric CT scanner (TOSHIBA, Japan). The patients received a D95 prescription of 50 Gy for PTV in 4 fractions. The single-arc VMAT with 6 MV was created by SmartArc in the Pinnacle v9.0 treatment planning system (Philips, USA). The constraint on MLC motion of 0.1 cm/degree was applied in the VMAT inverse plan so that MLC had little chance to hide the PTV. Such a constraint on MLC motion may significantly affect the quality of a treatment plan. Therefore, these plans were compared to those without constraints on MLC motion.

Treatment was performed by a single clockwise rotation (360 degrees). The arc used for reconstruction was from −180 to −19 degrees (patient 1) and from −180 to −40 degrees (patient 2). The angle range to allow portal imaging was limited by the Elekta iView software such that the maximum number of sequential acquisitions was 256. The difference between patients was due to the gantry speed determined by the VMAT plan.

Before applying the method to clinical cases, we conducted a 4D VMAT-CBCT reconstruction experiment by using the QUASAR respiratory motion phantom (Modus Medical Devices Inc.). The mechanical amplitude and cycle in the phantom were set at 10 mm and 3 s, respectively. The VMAT plan for patient 1 was delivered.

Result

VMAT plan with the MLC constraint

The dose-volume histograms (DVHs) for patients 1 and 2 are shown in Fig. 2a and b, respectively. The solid curves denote the DVHs with an MLC constraint of 0.1 cm/degree, while the dashed curves denote DVHs without MLC constraints. The dose homogeneity of the plan without MLC constraint was better than the plan with MLC constraint for both patients. Dose conformity was

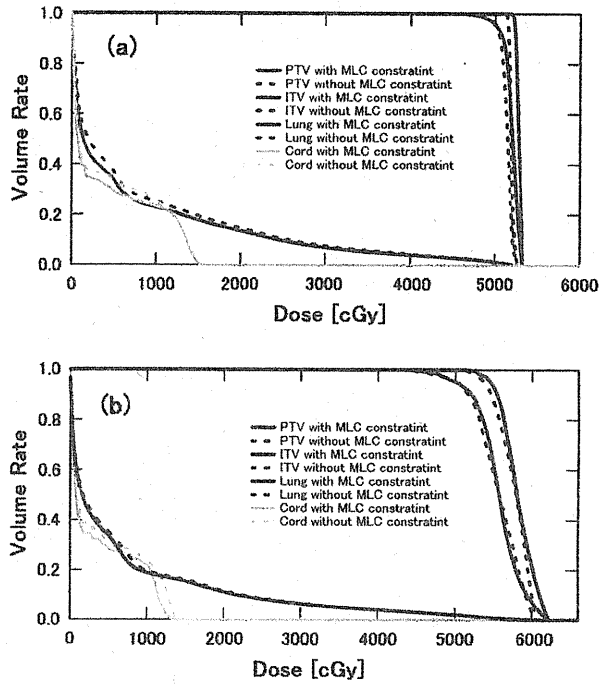

Fig. 2. DVH with and without MLC constraints for (a) patient 1 and (b) patient 2. All plans were prescribed as D95 of PTV equal to 50 Gy. The solid curves denote the DVHs with MLC constraint of 0.1 cm/degree, while the dashed curves denote those without MLC constraint.

comparable. On the other hand, the DVHs for organ at risk (OAR) with MLC constraint were slightly better than the DVHs without MLC constraint. This is presumably because in inverse planning, the constraint on homogeneity and conformity for PTV was stronger than the DVH constraint on OAR.

We found little difference between the plans with and without MLC constraints in the tested patients. The plans with MLC constraints were acceptable for clinical use and the MLC constraint was judged to manage the target motion without significant degradation of plan quality.

Acquisition of respiratory signal

The respiratory behaviours of two patients assessed by our P-IBPR method are shown in Fig. 3a and b. The original signal could have pseudo periodic components, such as those generated by gantry rotation. These components were removed by the band pass filter and, as seen in Fig. 3c and d, the motion due to patient respiration was clearly dissolved in all gantry angle directions. In Fig. 4, the breathing cycles were compared with those derived from the tumour motion in visual tracking. In Fig. 4a and b for patient 1, the breathing cycle was estimated by 3.7 ± 0.4 (1 SD) for both P-IBPR and visual tracking, while in Fig. 4c and d for patient 2, the breathing cycle was estimated by 2.7 ± 0.3 (1 SD) and 2.7 ± 0.4 (1 SD) for P-IBPR and visual tracking, respectively. The result in P-IBPR was concordant with the result of visual tracking. The difference of breathing cycle between P-IBPR and visual tracking was one sampling time (0.46 s) at most.

Reconstruction of 4D VMAT-CBCT in phantom

The reconstruction images of 4D VMAT-CBCT with an FBP algorithm corresponding to the points of maximum oscillation are shown in Fig. 5a and b. The standard calculation time for reconstruction with 270 × 270 × 80 voxels was about 10 s by GPU using